TR 93-05

AD-A268 871

REPOR

Form Approved
OMB No. 0704-0188

1. AGENCY USE ONLY (Leave blank)	2. REPORT DATE	3. REPORT TYPE AND DATES COVERED
	Feb 1993	Final Technical 30.9.90-31.12.92.

4. TITLE AND SUBTITLE

Metal Film Surface Plasmon Resonance (MFSPR) Fibre Couplers

5. FUNDING NUMBERS

(2)

G/AFOSR-90-0353
PR/4351/00

6. AUTHOR(S)

P.St.J. Russell and S. Barcelos

7. PERFORMING ORGANIZATION NAME(S) AND ADDRESS(ES)

Optoelectronics Research Centre,
University of Southampton,
Hampshire, SO9 5NH, UK.

8. PERFORMING ORGANIZATION REPORT NUMBER

9. SPONSORING/MONITORING AGENCY NAME(S) AND ADDRESS(ES)

EOARD
223/231 Old Marylebone Road
London NW1 5TH, UK.

10. SPONSORING/MONITORING AGENCY REPORT NUMBER

11. SUPPLEMENTARY NOTES

This document has been approved for public release and sale; its distribution is unlimited

12a. DISTRIBUTION/AVAILABILITY STATEMENT

93 8 23 074

93-19581

13. ABSTRACT (Maximum 200 words)

The project goal was to develop a mode selective coupler, based on long-range surface-plasmons (LRSP's), that provides tunable tapping of individual modes or small groups of modes from a multi-mode fibre carrying several communications channels simultaneously in different areas of its mode spectrum. When a thin metal layer, deposited on a side-polished fibre, supports a LRSP that phase-matches to a fibre mode, resonant tunnelling of light from the core into the metal layer can occur; this may then be tapped off through a high index prism (or a second identical fibre) placed against the fibre face, the intervening space being filled with a layer of variable index. Mode selectivity might then be achieved by tuning the index of this layer. In the project, the fibre side-polishing apparatus was designed and built; the polishing procedure perfected; a fully automated computer-driven prism coupler and monochromator set up; and reliable film deposition achieved. The theory of the LRSP modes was fully developed, and a separate field matrix analysis carried out for modelling the behaviour of the entire device both for excitation from the prism and the fibre modes. The general conclusion is that the modal selectivity is fundamentally limited by the unavoidable fact that higher order modes (those close to cut-off) couple much more strongly than do lower order modes. The result is that lower order modes cannot be coupled out without a substantial (of order 50% or worse) amount of cross-talk from higher order modes. These observations were confirmed in a number of experiments.

14. SUBJECT TERMS	15. NUMBER OF PAGES
Optical Fibres/Surface Plasmon-Polaritons/mode selective couplers	49
	16. PRICE CODE

17. SECURITY CLASSIFICATION OF REPORT	18. SECURITY CLASSIFICATION OF THIS PAGE	19. SECURITY CLASSIFICATION OF ABSTRACT	20. LIMITATION OF ABSTRACT

This report has been reviewed and is releasable to the National Technical Information Service (NTIS). At NTIS is will be releasable to the general public, including foreign nations.

This technical report has been reviewed and is approved for publication.

PARRIS C. NEAL, Lt Col, USAF
Chief, Aerospace Electronics

RONALD J. LISOWSKI, Lt Col, USAF
Chief Scientist

METAL FILM SURFACE-PLASMON RESONANCE (MFSPR) FIBRE COUPLERS
AFOSR 90-0353

Final Report – February 1993

P.St.J. Russell and S. Barcelos

Optoelectronics Research Centre,
University of Southampton,
United Kingdom
Tel +44 703 593083/Fax +44 703 593149

CONTENTS

1. SUMMARY

The project goal was to develop a mode selective coupler that provides tunable tapping of individual modes or small groups of modes from a multi-mode fibre carrying several communications channels simultaneously in different areas of its mode spectrum. The idea was that this might be achieved by depositing a thin metal layer on a side-polished fibre and arranging that the long-range surface plasmon (LRSP) mode is phase-matched to a fibre mode. Under this condition, resonant tunnelling of light from the core into the metal layer occurs; this may then be tapped off through a high index prism (or a second identical fibre) placed against the fibre face, the intervening space being filled with a layer whose refractive index may be varied. Different fibre modes might then be tapped off by altering the index of this layer, i.e., by altering the phase index of the plasmon mode. In the experiments: the fibre side-polishing equipment was designed, built and set up; the polishing procedure perfected; a fully automated computer-driven prism coupling apparatus built; a computer driven monochromator set up to provide tunable light for characterizing the LRSP resonances; accurate film deposition achieved; and a number of devices made and tested. On the theoretical front, reliable solutions of the LRSP dispersion relation were routinely obtained for any combination of parameters, and a separate field tunnelling analysis was developed for assessing the modal selectivity of the devices. The general conclusion is that the degree of modal discrimination is fundamentally limited by the unavoidable fact that higher order modes (those close to cut-off) couple much more strongly than do lower order modes. This is because the evanescent tailing field rapidly extends further out into the cladding as the modes approach cut-off, i.e., as the modal rays approach the critical angle at the core-cladding interface. The result is that lower order modes cannot be coupled out without a substantial (of order 50% or worse) amount of cross-talk from higher order modes. These observations are confirmed in a number of experiments.

2. STATEMENT OF WORK

2.1 Introduction

Prior to the present project, highly polarization-selective devices had been demonstrated in single-mode optical fibre using the optical/surface plasmon interaction. This interaction depends on meeting the correct phase-matching conditions for LRSP propagation along a thin metal layer. This condition is satisfied when the LRSP phase index matches the phase index of the guided mode in the fibre. The LRSP index is dependent on the geometrical form of the guiding structure, the refractive index of the dielectric layers, the dimensions of each layer, the optical wavelength and the metal used. Precise matching produces a resonance condition at which light is resonantly coupled from the fibre mode to the LRSP mode. This resonance condition, which under certain design conditions has very high finesse, can also be used to select specific propagation constants in a multi-mode fibre. The aim of the research project was to explore whether an effective mode-selective fibre output coupler could be built based on this idea. The envisaged application was to modal-division multiplexing, each group of modes selected by a (tunable) LRSP resonance acting as a separate channel in a short-haul communications link.

The program of work involved investigating the modal selectivity properties of thin metal overlays on polished multi-mode optical fibre. The fibre ultimately to be investigated was Corning type 5 using a 0.82 μm LED. In order to understand more clearly the mode selection process, we also worked extensively with a dual-mode fibre at 632.8 nm. Access to the evanescent field of the fibre was achieved by using the side-lapping/polishing technique developed for single-mode tunable couplers and in-line grating devices.

Several parameters were investigated for these devices including the interaction length and polishing depth for optimum modal selectivity and efficiency. The research was conducted with a dual approach, modelling and designing the device theoretically and then confirming the analysis through practical experimentation. The next three sections are extracted from the original Statement of Work.

2.2 Task 1: Modal Selectivity

Each of the modes guided in a multi-mode fibre propagates at a unique phase velocity with different degrees of evanescent penetration into the cladding. Therefore the boundary conditions to create surface plasmon waves in the metal are different for different modes or groups of modes. The interaction is highly polarization selective and will therefore only affect part of the propagation even in highly interactive situations. Plasmon mode interaction is governed by the same wave equations (Maxwell's equations) and consequently coupling conditions as any other guided wave. For a simple structure it can be considered that energy is coupled periodically between the plasmon waves and the fibre during the process. The

selectivity will be dependent on the field overlap between the plasmon and fibre modes and the interaction length. Two critical parameters to be investigated under this task are the effects of different interaction lengths and polishing depths on modal selection. Different radius curves in the substrate supporting the fibre will be used and various polishing depths investigated. Aluminium, Silver and Gold films will be investigated. The film thickness is also a critical parameter in the generation of particular plasmon modes and will be studied.

The objective of task 1 is to define reliably the modal selectivity in such a way that particular groups of modes can be selected by correct choice of fabrication parameters.

2.3 Task 2: MFSPR coupler efficiency

Once the modal selectivity has been shown and characterized the next stage will be to collect the light coupled to the surface plasmon mode in a second side-polished fibre. This is analogous to the single-mode fibre polarizing beam-splitter which generates surface plasmon modes for one polarization and couples them to a second fibre. Once again several parameters must be considered to optimise the modal selectivity and power cross-coupling. The waveguiding structure is of critical importance. Different glasses (and other materials) of varying hardness will be used for the mounting blocks in order to fine-tune the position of the polished fibre-face relative to the block surface. This will enable control of the closeness of the two polished fibre faces in the coupler structure. The second fibre is an integral part of the guiding structure and its presence modifies the characteristics of the single device. The parameters to be investigated will be the matching dielectric thickness between the fibres, the possible use of a second thin metal layer and the relative overlap of the interaction areas. The critical parameter for this device will be the losses imposed which relates to the efficiency defined in the task outline.

2.4 Task 3: Switching times for MFSPR

The first two tasks are aimed at defining and optimising the mode selective coupler using surface plasmon interaction. The third task is to investigate the switching possibilities in such devices. Three possible approaches can be considered for switching the devices; liquid crystal, thermal or piezo-electric. The thermal route would involve design of suitable electrodes, possibly using the metal film itself as the heating element. Switching times of 100's of μsec should be possible in this case (limited by thermal conductive cooling). The piezo-electric alternative is more attractive as regards speed of switching; the fibre could be mounted in a groove cut in a piezo-electric transducer, or the coupler spacing varied by means of three piezo-electric pads spacing the two blocks. This would permit switching by modulation of the inter-fibre spacing. The thermal route would permit switching via temperature-related changes in dielectric constant and inter-fibre spacing. The liquid crystal alternative would involve placing a layer of nematic (perhaps ferroelectric) liquid crystal between the upper coupler face and the metal layer; this would require the deposition of an aligning layer and a transparent electrode on the upper fibre face, the effect of which on the LRSP resonance would need to be assessed. Switching speeds of ferroelectric LC's could be

of the order of 10-100 nsec.

3. DESCRIPTION OF WORK CARRIED OUT

3.1 Production of polished metal-coated half-coupler blocks

The block preparation, groove cutting, fibre gluing, side-lapping and polishing procedures were perfected for multi-mode, few-moded and single-mode fibres. The polishing depth, and hence strength of interaction, could be closely controlled. The work involved designing and building a special high-precision sawing apparatus for variable-radius groove cutting (Figure

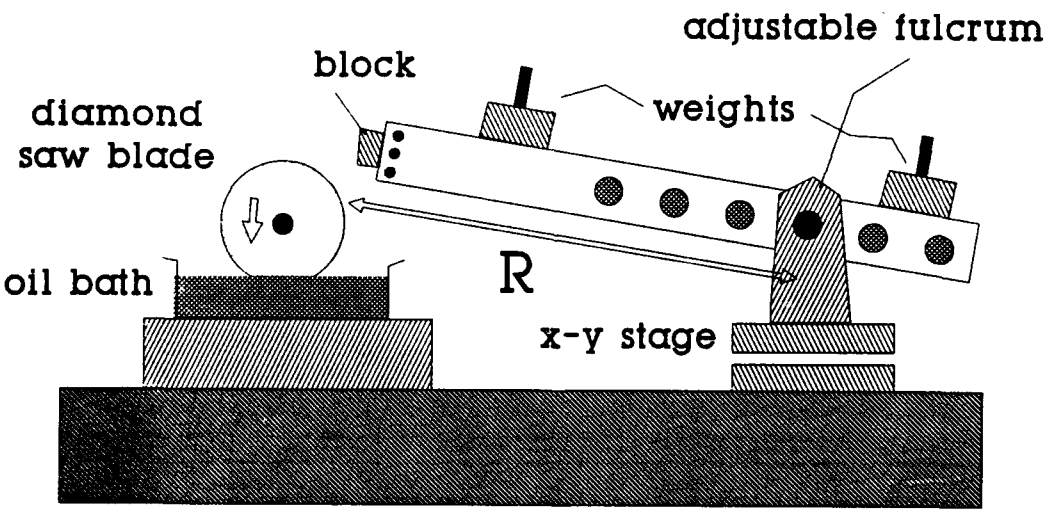

Figure 1: Saw for cutting grooves in glass mounting blocks; the radius of curvature of the groove equals the length of the rotating arm

1), and a device for precise positioning and gluing of the stripped fibre under tension in the curved groove (Figure 2). For maximum hardness, the epoxy resin used to bond the fibre into the groove was cured at 100°C in an oven.

Sergio Barcelos attended a three-day training course in optical polishing at LogiTech, the company that supplied the polishing equipment, and subsequently mastered the intricacies of the lapping/polishing procedure. Of critical importance in the process is tight and accurate control of the distance between the polished surface and the evanescent field of the guided modes. We initially tried the oil drop technique (Figure 3) developed at Stanford [D2,D3,D5]. This relies on the fact that light leaks out of the core at a rate strongly

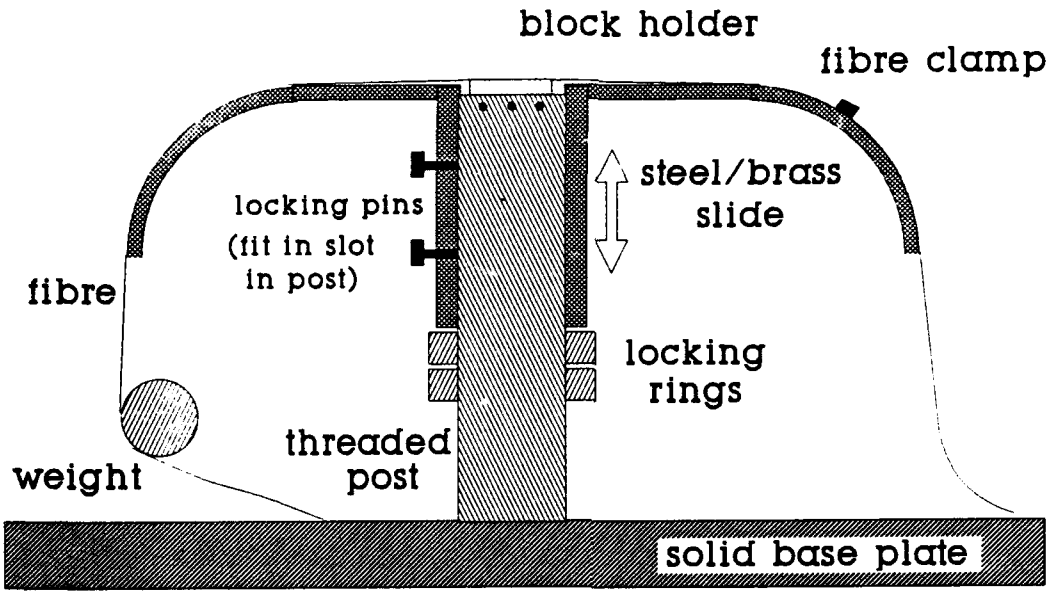

Figure 2: Gluing jig; the fibre is held securely under tension, stripped of its plastic cladding, and placed precisely along the bottom of the groove

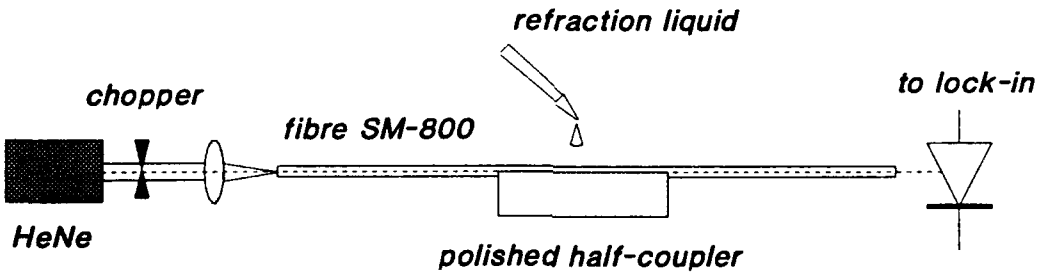

Figure 3: The oil-drop technique: The proximity of the core during polishing is determined by the attenuation in transmission measured after placing a drop of oil (index just below that of the guided modes) in the evanescent field

dependent on the index of the oil and its distance from the field of the guided mode. Although it works in a repeatable and precise manner for single-mode fibres, interpretation of the results is more complicated when multi-mode fibres are used because different modes have different penetration depths (see Figure 4 for our results on dual-mode fibre). For comparison with the multi-mode devices, and to gain confidence in LRSP characterization techniques, several single-mode side-polished coupler halves were also prepared.

For the mathematical modelling in section 3.4, it is essential to know accurately the distance

between the polished surface and the edge of the core. In order to measure this directly, a number of dual-mode fibre blocks were cut in two and polished, and examined in both an optical and a scanning electron microscope. Photographs of the resulting block cross-section are given in Figure 5, where the position of the core is clearly visible.

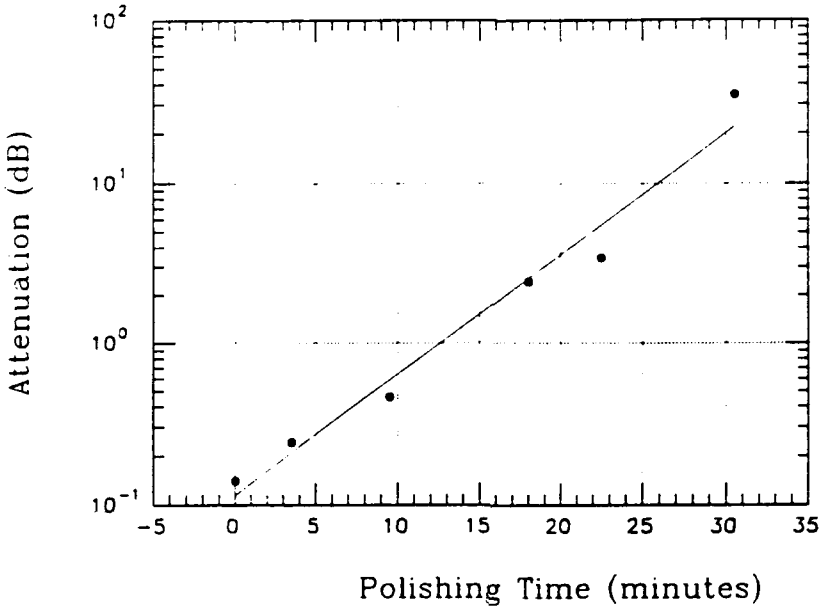

Figure 4: Attenuation versus polishing time for dual-mode fibre; time zero corresponds to the onset of measurable attenuation using the oil-drop technique

The use of paraffin or light mineral oil for suspending the polishing powder (cerium oxide) was investigated. Because the higher index of the oil permits stripping of the fibre modes once the core is reached, real-time monitoring of polishing quality is then possible, permitting more rapid production [D7]. It was decided to halt the implementation of this automated lapping and polishing process because perfecting the technique was proving more time-consuming than initially expected, and concentrating on it would have slowed down progress on the program as a whole.

A vacuum evaporator was used for film growth, and the film thickness calibrated against absolute measurements using a Tencor profilometer. The deposition accuracy achieved was normally within ± 3 nm of the target thickness for both aluminium and silver.

3.2 Fibre characterization by prism coupling

A prism coupling rig was built for characterizing the mode spectrum of the fibre, and fully automated using a computer-driven turn-table. Small groups of modes – even single modes

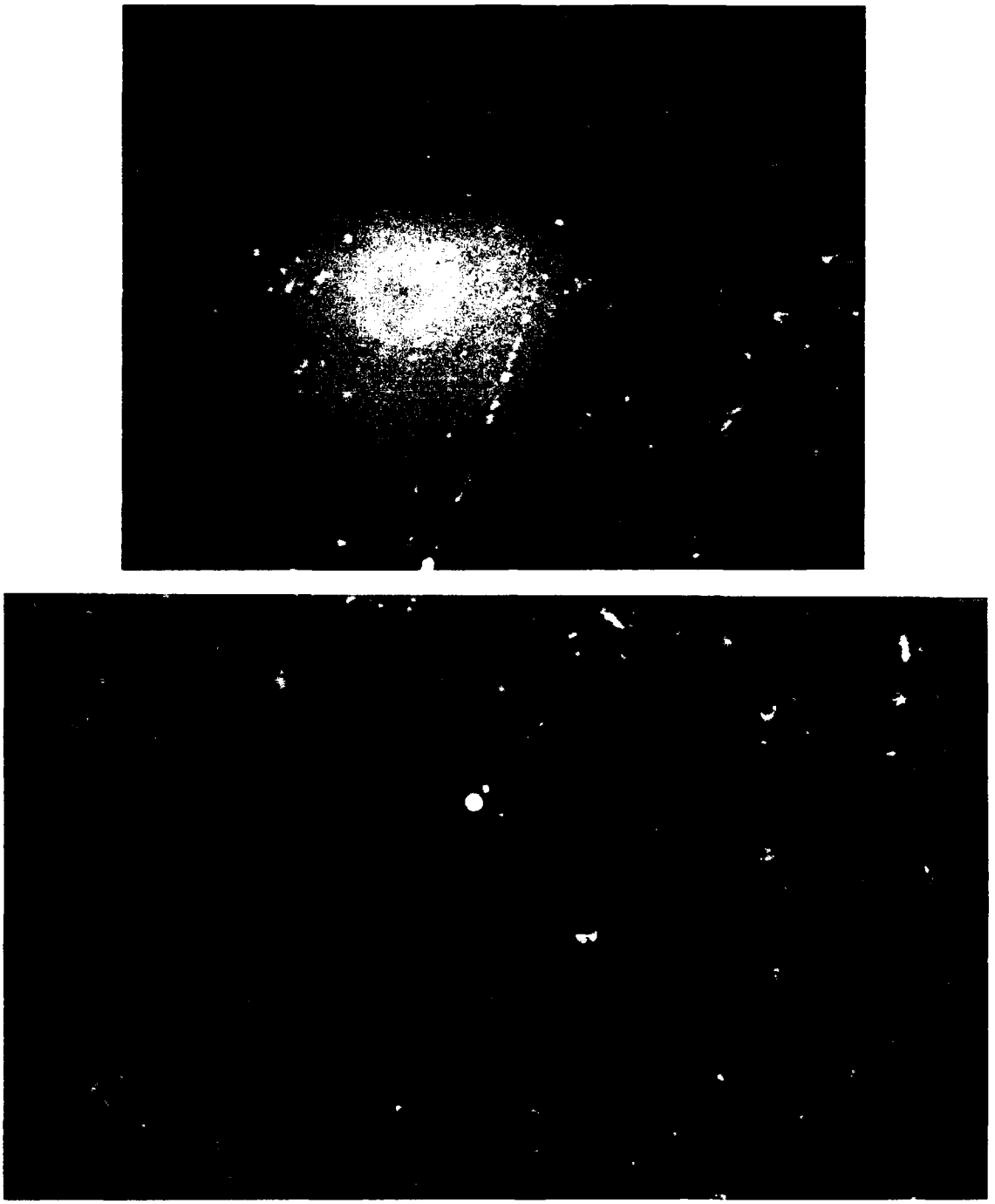

Figure 5: Photographs of dual-mode fibre blocks cut in two and examined in an electron microscope. The upper photograph was taken in a scanning electron microscope, and the lower on in an optical microscope; the core (3 μm in diameter) is clearly visible in each case.

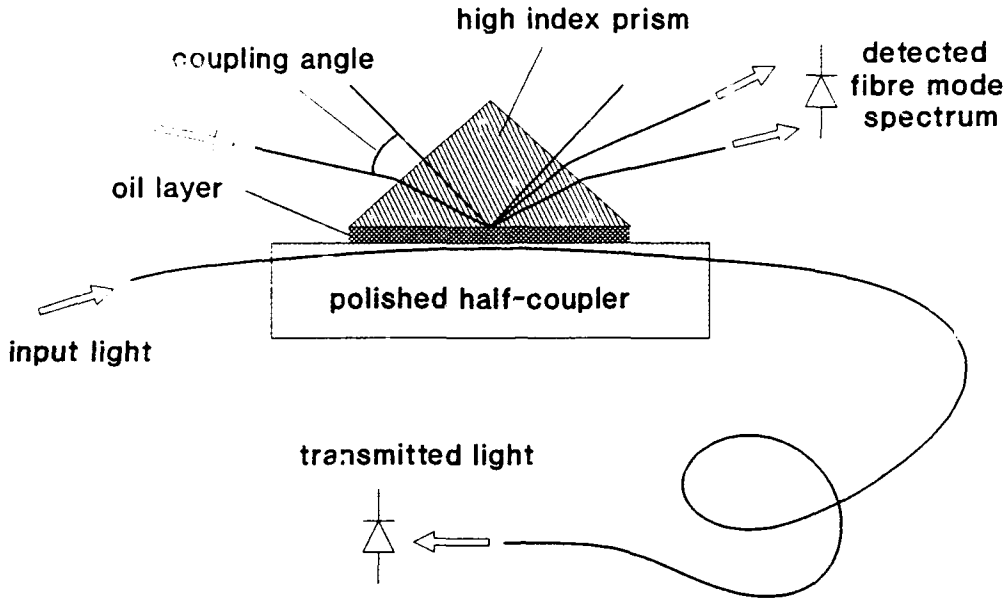

Figure 6: Prism coupling technique; both input and output coupling are illustrated. The coupling angle (between the normal and the incident ray) is geometrically related to the effective index of the excited mode

– could be excited routinely in the fibre using this technique, and the modes already present in a fibre could be identified by analyzing the angular spectrum of the light coupled out by the prism. The technique is illustrated in Figure 6. A high index coupling prism is placed close to the side-polished fibre surface, a layer of index oil ($n_{oil} < n_{mode} < n_{prism}$) in between where n_{mode} is the effective phase index of any one of the fibre modes. At the correct angle of incidence, light is able to tunnel through the intervening layer of oil and appear as a single guided mode (or group of modes) in the fibre core. The angular range over which such coupling is possible can be simply related to the spread of effective indices where guided modes appear, providing direct measurement of a parameter essential in the design of the device. The results of prism coupling for the Corning 50/125 CPC3 multi-mode fibre used in the project are presented in Figure 7. Initially to gain experience with the prism-coupling technique, but later adopted extensively to study mode selection, experiments were carried out on a fibre that is two-moded at 633 nm (LP_{11} cut-off wavelength 800 nm; V–value 3.04 at 633 nm). To confirm the accurate operation of the prism coupler, two half-coupler blocks were prepared using this fibre. The first (Block #11) was polished until the attenuation induced by the oil-drop technique (see Figure 3) for n_{oil} = 1.472 was 31 dB, and the second (Block #12) until the attenuation was 44 dB.

In order to check the accuracy of our experimental measurements of the phase index in the

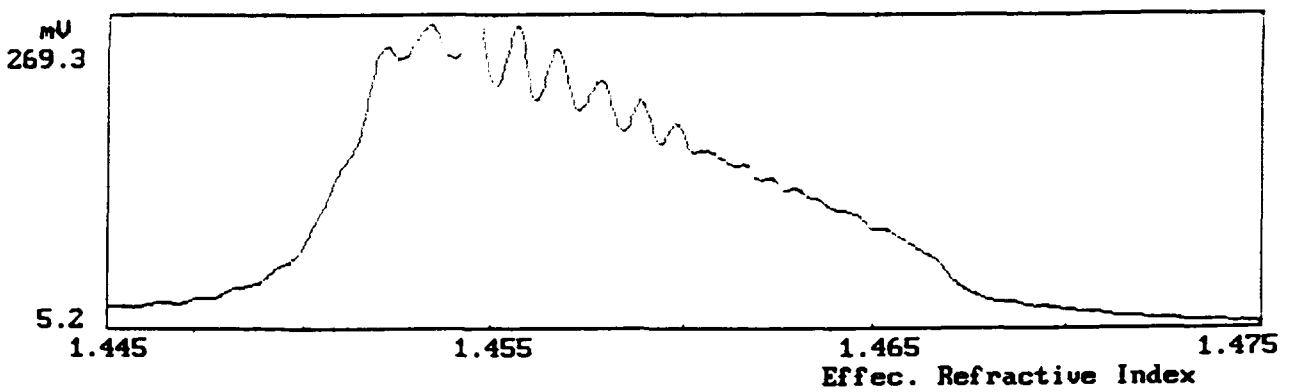

Figure 7: Mode spectrum (measured by prism coupling) of multi-mode fibre; the mode indices range from 1.450 to 1.467 (the cladding has a depressed index due to F-doping). This data is needed for designing the mode selective coupler; the ripple is caused by polarisation effects

dual-mode fibre, we compared three different techniques. In the first, light was prism coupled into the fibre in Block #12 and the transmitted power monitored at the fibre end. An oil of refractive index less than the LP_{11} mode index was used between the prism and the polished fibre face. The data is plotted in Figure 8, where the effective indices of the LP_{01} and LP_{11} modes are readily measured to be $n_{11} = 1.4620$ and $n_{01} = 1.4685$. In the second experiment, light was launched into the fibre and coupled out by the prism, which as before was placed against the polished fibre face (Block 12) with index oil in between. After measuring the exit angles of the out-coupled beams from the two modes in the fibre, the

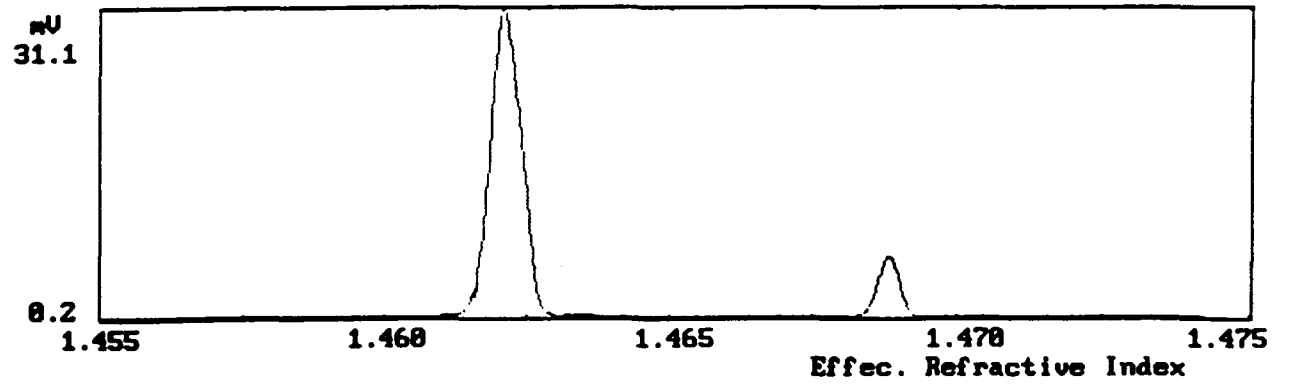

Figure 8: Results of prism coupling into dual-mode fibre; both modes are found, and owing to the greater penetration of its evanescent field into the oil (see Figure 22), the LP_{11} mode is more strongly excited than the fundamental LP_{01} mode

effective indices of the guided modes were calculated to be $n_{01} = 1.4674$ and $n_{11} = 1.4620$. Finally, using the oil drop technique (Figure 3) on Block #12, we obtained the data in Figure 9. The refractive indices that cause stripping out of the LP_{11} and LP_{01} modes agree quite well with the results of the first two measurements. The results from the three experiments agreed to within $\pm 0.05\%$.

3.3 LRSP characterization techniques

Just as for the fibre mode spectrum, the main technique used for characterizing the LRSP resonances is prism coupling. Light of the correct polarization (TM or *s*-polarised for LRSP excitation) is launched, via an overlay of oil, directly into the LRSP mode of the metal layer. Once the correct angle for excitation of a LRSP mode is met, a dip appears in the reflected power owing to coupling into the LRSP mode. The strength of this dip will be reduced if the focused laser beam is intercepted only partly by the core; it will also be broadened by the presence of the cladding, epoxy and block surfaces where other LRSP resonances will occur for different values of index. If at the same time the LRSP mode above the core phase-matches to a fibre mode (or in the multi-mode case to a small group of modes), the amount of light coupled into the core will be enhanced. If the LRSP resonance condition is not fulfilled, some tunnelling can occur owing to simple field penetration through the metal layer, which cannot completely exclude light (the 1/e skin depth is never zero). The process is one of frustrated total internal reflection, through the index oil, into the metal film and thence into the fibre. The technique is very versatile, permitting measurements of the dependence of the resonances on wavelength and superstrate index. Since any coupling out of the TE mode is undesirable, it is of importance to be able to investigate the behaviour for TE polarisation; this may be done simply by rotating the polarization state of the incoming light through 90°.

The exact position of the LRSP resonance depends on the index of the oil, the thickness of the metal layer and the particular metal used. The values of all these parameters must therefore be carefully chosen (see theory section). The amount of light coupled into the fibre (or out of it in the reverse process) depends on the modal overlap between the evanescent tail of the field below the prism and the LRSP mode, and the overlap between the fibre mode and the LRSP mode on the lower side of the metal film. The strength of the interaction can be tuned by varying the polishing depth into the fibre and the prism/metal spacing.

To facilitate detailed and reproducible measurements, the stepping-motor driven prism coupling turn-table and the monochromator/white light source were fully automated for computer control, using software written in the Quick-Basic environment. The automated prism coupling turntable uses an accurate referencing technique first suggested in [D15]. Depending on the light source used, the monochromator is able to deliver tunable narrow-band radiation from 167 nm to 1500 nm. The systems were fully operational and fully capable of producing reliable measurements on the prototype devices – see Section 3.6.

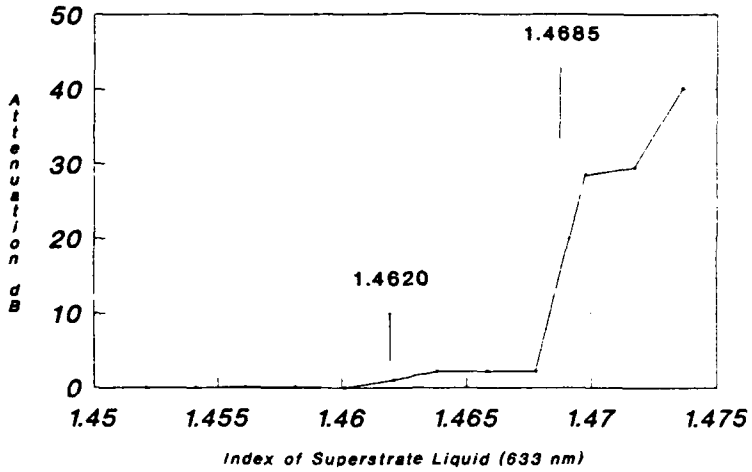

Figure 9: Attenuation versus superstrate oil index for a polished dual-mode fibre at 632.8 nm; note the sharp onset of loss for the LP_{01} (at 1.4685) and LP_{11} (at 1.4620) modes

3.4 Theoretical modelling

3.4.1 Summary

Two main areas of theory were successfully addressed. These are, first, solutions of the dispersion relation for coupled surface plasmon-polaritons on thin metal films, and second, a multi-layer field-matching procedure for analyzing prism coupling and finding the normal modes of the whole fibre/film/prism composite structure. Both mathematical problems have been programmed in IBM's APL2 language (on a PC486/33 MHz machine), and yield reliable solutions in all parameter ranges. The authors are willing to provide the source codes if requested. The two analyses led to considerable clarification of the operation of the devices, permitting us to explain the experimental behaviour reliably.

3.4.2 Solutions to the dispersion relation

The film geometry is sketched in Figure 10. The basic problem solved was the numerical solution of the transcendental equation [A1,A3,A6,A7]:

$$\begin{aligned} \tanh(hQ_2)\left(\epsilon_2\epsilon_4 Q_3^2 + \epsilon_m^2 Q_2 Q_4\right) + Q_3\epsilon_3\left(\epsilon_2 Q_4 + \epsilon_4 Q_2\right) &= 0 \\ Q_n &= S_n\sqrt{\{\beta^2 - \epsilon_n k_v^2\}}, \end{aligned} \tag{1}$$

k_v is vacuum k-vector, $\epsilon_2 = n_2^2$, $\epsilon_4 = n_4^2$ and $\epsilon_3 = \epsilon_m = \epsilon_{mR} + j\epsilon_{mI}$

where β is the modal propagation constant. In the definitions of Q_n, the sign of the square root is always chosen so that its real part is positive; the overall sign of Q_n is then determined by S_n. It is found in the analysis that bound modes appear when $(S_4,S_2) = (+1,+1)$. Leaky and growing modes appear when if either S_4 or S_3 is negative (both bound and leaky modes are characterised by having a propagation constant β with a negative real part, whereas growing modes it is positive). Parameter ranges exist (such as in Figure 11) where two leaky and two bound modes exist, i.e., $(S_4,S_2) = \{(-1,+1), (+1,+1)$ and $(+1,-1)\}$ all yield solutions, the bound case $(+1,+1)$ yielding two solutions. Other

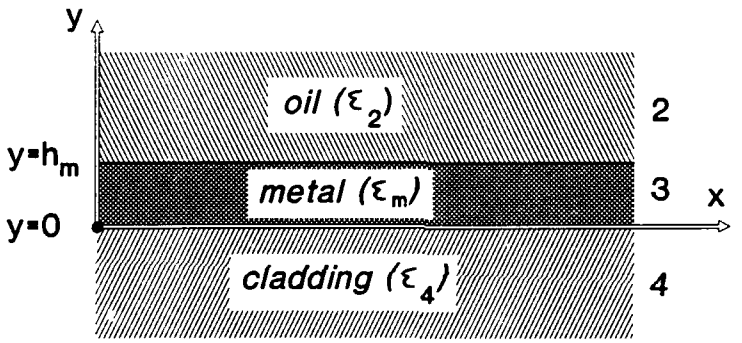

Figure 10: Metal film geometry for long range surface plasmon dispersion relation

parameter ranges exist (see the higher and lower ranges of n_2 in Figure 12) where two leaky, one bound (the anti-symmetrical or high-loss one) and one growing mode exist, i.e., $(S_4,S_2) = \{(-1,+1), (+1,-1)$ and $(+1,+1)\}$, either the first or second combination yielding two solutions (one leaky and one growing). If $\epsilon_4 > \epsilon_2$, $(S_4,S_2) = (-1,+1)$ yields either a leaky plus a growing mode or just a leaky mode. If $\epsilon_4 < \epsilon_2$, then it is the combination $(S_4,S_2) = (+1,-1)$ that yields this. It is clear, therefore, that the nature of the four solutions depends on the parameter range being investigated [A3].

Some illustrative results are plotted in Figures 11 and 12. In each figure the dependence of the phase and attenuation indices on superstrate index is explored, first of all (Figure 11) for a 26 nm thick silver film at 632.8 nm and secondly (Figure 12) for a 25 nm thick silver film at 827 nm. In each case the substrate index is 1.457, i.e., close to the cladding index in the fibres. Notice that the solutions tend, away from the resonance (given by the stop-band), to asymptotic values that correspond to uncoupled single surface plasmon polaritons on the two interfaces. The propagation constant β_n (n=4 or 2) of these modes is given by:

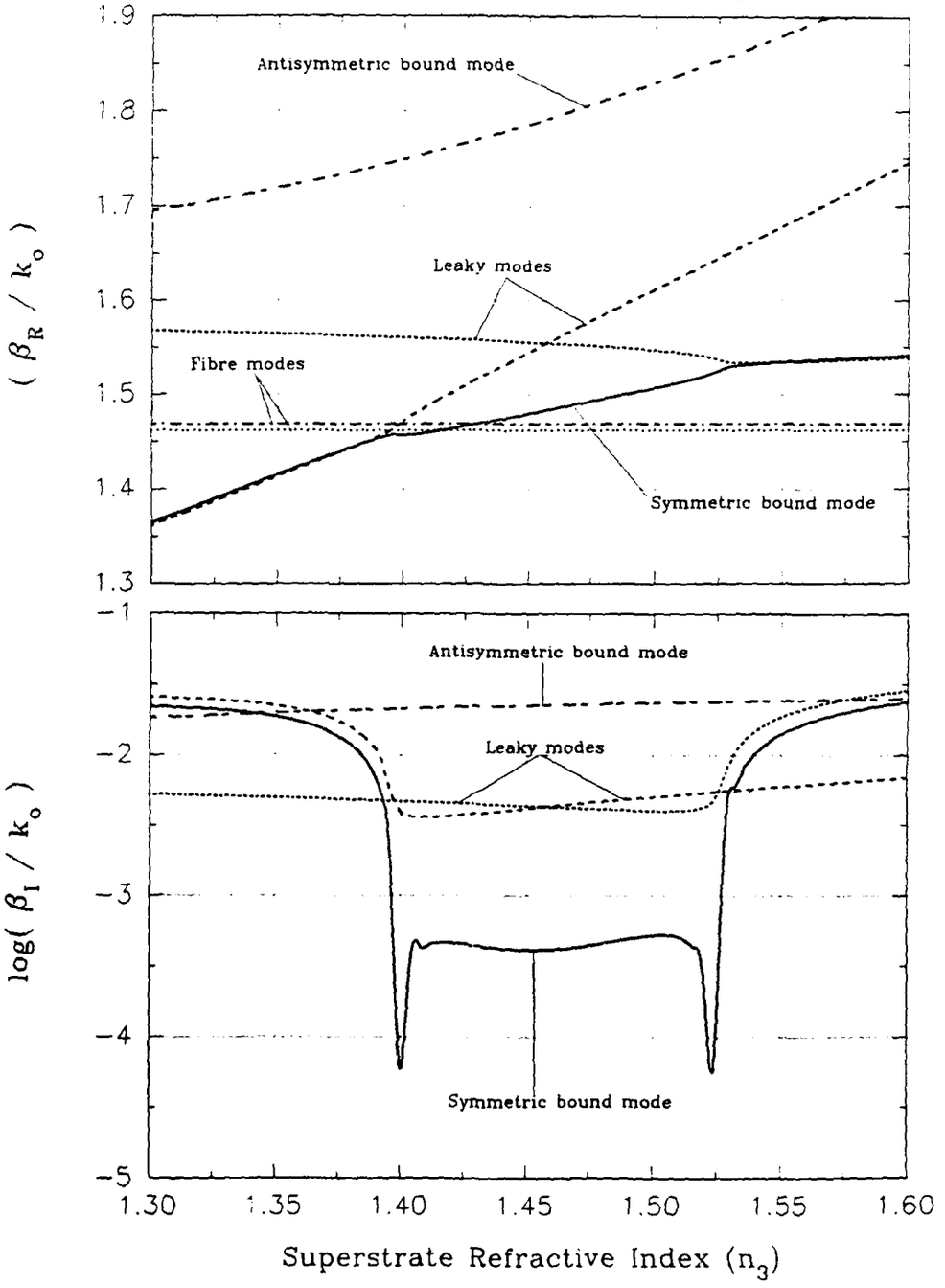

Figure 11: **Real (upper) and imaginary (lower) parts of the effective index of the coupled surface plasmon modes, plotted against superstrate index n_2, at λ = 632.8 nm on a 26 nm thick layer of silver ($\epsilon_m = -17.5 - j0.7$) for a substrate index of 1.457**

$$\beta_n = k_o \sqrt{\{\epsilon_n \epsilon_m / (\epsilon_m + \epsilon_n)\}} \quad (2)$$

The appropriate operating point for good mode selection is at the lower edge of the asymmetric bound (LRSP) range where the attenuation is very low and the refractive indices of the LRSP modes are close to the indices of the fibre modes (also marked in the figures). Notice in particular that the low-loss resonance region (where symmetric bound modes with decaying field amplitudes are excited) exists only for a limited range of superstrate indices (Figure 12). This range shrinks in extent (and the LRSP loss falls) as the film thickness is reduced.

3.4.3 Device operation and modal selectivity

The conclusions of this section differ from the preliminary ones presented in the Annual Report, where the complete analysis had not yet been carried out. We present the full field analysis, which shows that, even in the dual-mode fibre device, the mode discrimination is limited. The reason is that the evanescent tailing fields, whose penetration depth is a strong function of fibre mode index (it approaches infinity at the critical angle, i.e., at cut-off), dominates the behaviour of the device. The analysis uses a field matrix approach, which permits both excitation from the prism and the fibre to be treated. In the latter case, the normal modes of the whole structure are found and then used to model the evolution of the fields with distance along the coupler for excitation by a single mode of a dual or multi-mode fibre.

The geometry used is sketched in Figure 13. We make the approximation that the fibre core can be represented by a planar waveguide; this greatly simplifies the analysis while not greatly affecting its conclusions (with the exception of the polarisation properties – see the experimental multi-mode results, Figures 28-31). A number of approaches are possible to solve the field matching problem. The one adopted here is the set up the full matrix describing all the fields present in the structure. The general electric field in the nth layer is taken in the form:

$$\mathbf{E}_n = \{\mathbf{I}_n \exp[-j\gamma_n(y - y_n)] + \mathbf{R}_n \exp[j\gamma_n(y - y_n)]\} \exp(-j\beta x) \quad (3)$$

$$\gamma_n = \sqrt{(k_v^2 \epsilon_n - \beta^2)}$$

where for TM (p–polarised) light the field amplitudes $\mathbf{I}_n$ and $\mathbf{R}_n$ have zero z components, and for TE (s–polarised) light they point parallel to z. It is easy to show that for the TM

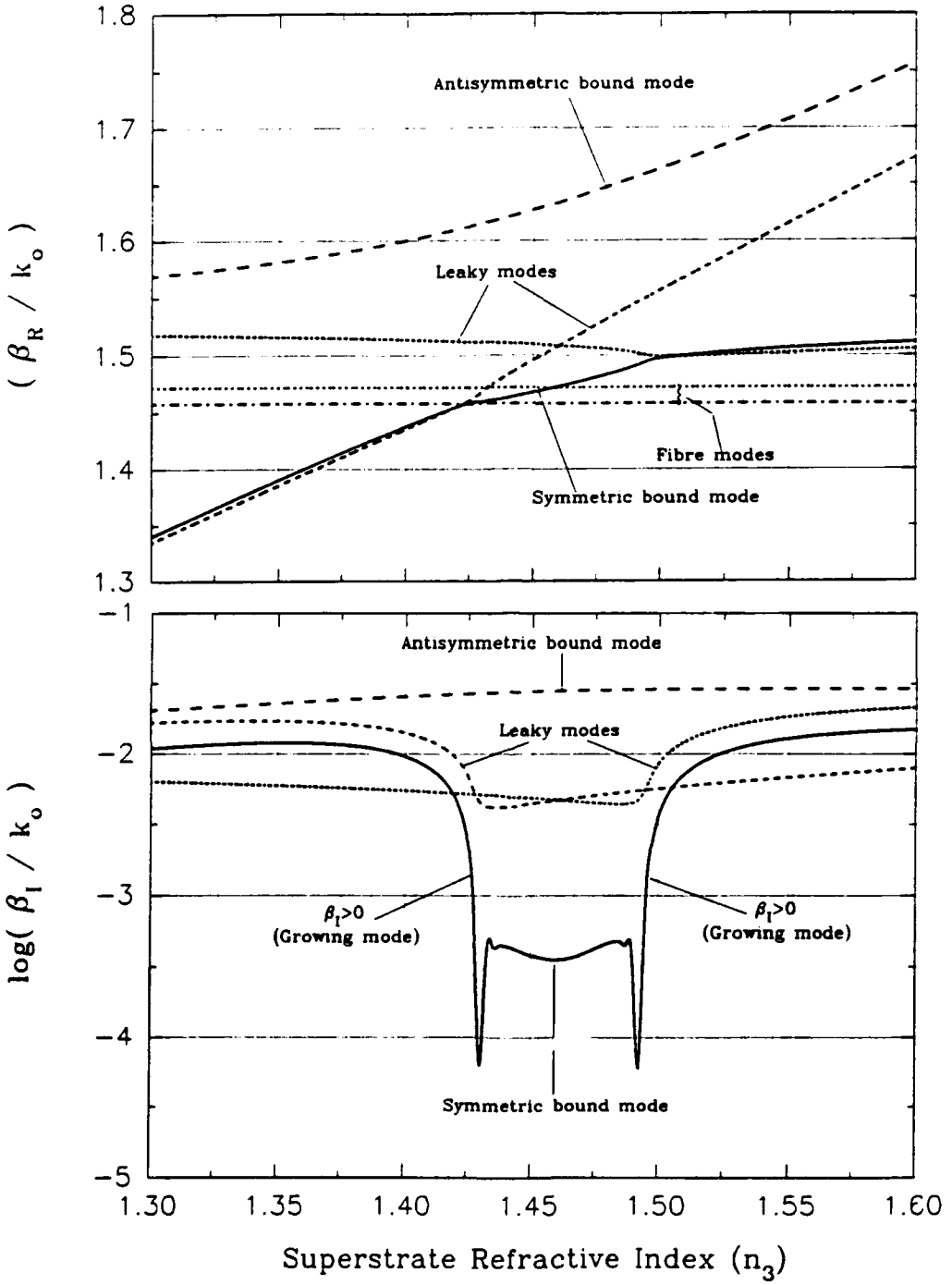

Figure 12: Real (upper) and imaginary (lower) parts of the effective index of the coupled surface plasmon modes, plotted against superstrate index n_2, at λ = 827 nm on a 25 nm thick layer of silver (ϵ_m = −33.5−j3.1 [E2]) for a substrate index of 1.457; note that the LRSP (symmetric bound) mode phase-matches to the multi-mode fibre modes in the range 1.425 < n_2 < 1.46

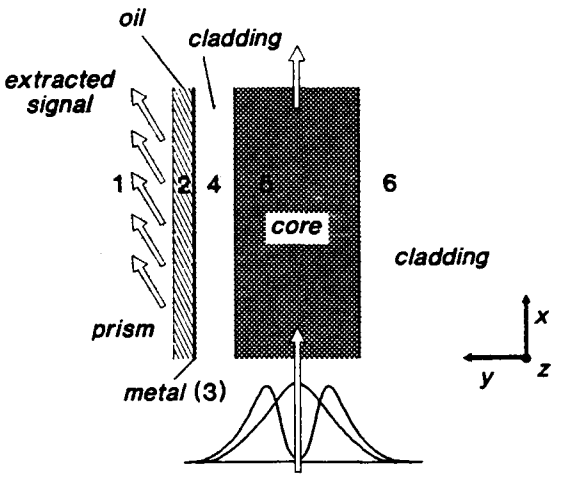

Figure 13: Geometry for field matching analysis; the structure is excited either at the prism/oil interface by a beam, or (as illustrated) by a fibre mode. In the general case, for arbitrary β values, some reflected and some transmitted light is generated. Under specific conditions (i.e., when the field matrix has a zero determinant), the wavevector β corresponds to that of an eigenmode of the structure.

case the x and y field components are related by:

$$I_{nx}/I_{ny} = -R_{nx}/R_{ny} = -\gamma_n/\beta \tag{4}$$

which halves the number of unknown field amplitudes. Defining a further parameter:

$$q_n = -\gamma_n - \beta^2/\gamma_n \tag{5}$$

we obtain the matrix equation in Figure 14, which takes the general form:

$$[\mathbf{M}]\{E_x\} = \{V_o\}. \tag{6}$$

This equation permits easy modelling of the behaviour of the fields for excitation a) through the prism and b) from the fibre. In case a) the column vector $\{V_o\}$ is directly related to the field incident on the base of the prism. In the second case the normal modes of the whole multi-layer composite structure are found by locating numerically the values of β for which the determinant of [M] is zero. These modes may then be superimposed to satisfy the boundary condition at entry to the coupler.

$$
\begin{pmatrix}
1 & -1 & -1 & 0 & 0 & 0 & 0 & 0 & 0 & 0 \\
-q_1 & -q_1 & q_2 & 0 & 0 & 0 & 0 & 0 & 0 & 0 \\
0 & e^{-j\gamma_2 h_2} & e^{j\gamma_2 h_2} & -1 & -1 & 0 & 0 & 0 & 0 & 0 \\
0 & q_2 e^{-j\gamma_2 h_2} & -q_2 e^{j\gamma_2 h_2} & -q_3 & q_3 & 0 & 0 & 0 & 0 & 0 \\
0 & 0 & 0 & e^{-j\gamma_3 h_3} & e^{j\gamma_3 h_3} & -1 & -1 & 0 & 0 & 0 \\
0 & 0 & 0 & q_3 e^{-j\gamma_3 h_3} & -q_3 e^{j\gamma_3 h_3} & -q_4 & q_4 & 0 & 0 & 0 \\
0 & 0 & 0 & 0 & 0 & e^{-j\gamma_4 h_4} & e^{j\gamma_4 h_4} & -1 & 0 & 0 \\
0 & 0 & 0 & 0 & 0 & q_4 e^{-j\gamma_4 h_4} & -q_4 e^{j\gamma_4 h_4} & -q_5 & 0 & 0 \\
0 & 0 & 0 & 0 & 0 & 0 & 0 & e^{-j\gamma_5 h_5} & e^{j\gamma_5 h_5} & -1 \\
0 & 0 & 0 & 0 & 0 & 0 & 0 & q_5 e^{-j\gamma_5 h_5} & -q_5 e^{j\gamma_5 h_5} & -q_6
\end{pmatrix}
\begin{pmatrix}
R_{1x} \\ I_{2x} \\ R_{2x} \\ I_{3x} \\ R_{3x} \\ I_{4x} \\ R_{4x} \\ I_{5x} \\ R_{5x} \\ I_{6x}
\end{pmatrix}
=
\begin{pmatrix}
-I_{1x} \\ -q_1 I_{1x} \\ 0 \\ 0 \\ 0 \\ 0 \\ 0 \\ 0 \\ 0 \\ 0
\end{pmatrix}
$$

Figure 14: Matrix equation for the multi-layer MFSPR coupler geometry

In the initial design stage, the simple procedure outlined in the previous section is followed. The LRSP mode phase index (in isolation) is matched to the index of the LP_{11} or the LP_{01} mode of the fibre (also in isolation). As is usual in coupled mode situations, each of these two modes combines with the LRSP mode to form two composite normal modes of the entire structure, which then are superimposed to satisfy the boundary condition at $x=0$. These composite modes are closely related to the "even" and "odd" modes well known from directional coupler theory; and although in some cases one or other of these normal modes is leaky or growing, the presence of two guided normal modes is practically guaranteed if the LRSP mode is matched to the fibre mode under consideration. By varying the degree of phase-matching between the LRSP and the fibre mode, the LRSP-like/fibre-like characteristics of the composite modes can be varied. For example, if most of the power in a normal mode is present in the LRSP region, the absorption will be high, whereas if most of the power is in the fibre, the absorption will be low. The normal mode in this second case is sometimes known as an *extended range* LRSP mode [ref].

The behaviour of these modes determines in very large measure the performance of the MFSPR coupler device. To illustrate the two methods of excitation (from the prism and through the fibre core) in the dual-mode fibre, the results of some numerical simulations are now presented.

3.4.3.1 Excitation through the prism: multi-mode case

First of all, in Figure 15 the magnetic field intensity ($|H_z/H_o|^2$) at the base of the prism and at the upper edge of a multi-mode core is plotted against n_{eff}; H_o is the incident magnetic field strength in the prism and the horizontal axis is the effective index of the incident light along the prism base. The oil, metal, cladding and core thicknesses are 1 μm, 26 nm, 5 μm and 30 μm, and the refractive indices of the oil, cladding and core are 1.418, 1.457 and 1.47066 respectively. The metal is silver, which has $\epsilon_m = -17.7 - j0.717$ at the operating wavelength of 633 nm. Notice the sequence of peaks, each corresponding to one of the 19 TM modes that the guide supports. Only qualitative conclusions can be drawn from the heights of these peaks – for example, there is a slight increase in the core field intensity in the region of the LRSP resonance. For quantitative estimates of the strength of coupling, a more highly developed theory must be used. One such theory, which turns out to be quite accurate, involves approximating each of the peaks by a Lorentzian absorption line in the form:

$$L(n_{eff}) = A_0 \left\{ \frac{\alpha}{\alpha - j(n_{eff} - n_{0m}} \right\} \qquad (7)$$

In this expression, n_{0m} is the value of index at which the absorption is maximum (usually very close to a mode index in the waveguide), n_{eff} the effective index of excitation, A_0 a scaling amplitude and α the Lorentzian absorption parameter. It may be shown that the values of β which are roots of det[**M**]=0 yield directly the parameters α and n_{0m} via the simple relationship $\beta = k_v(n_{0m} - j\alpha)$ where k_v is the vacuum wavevector. This means that the values of n_{0m} and α can be found for each resonance by solving the determinantal problem

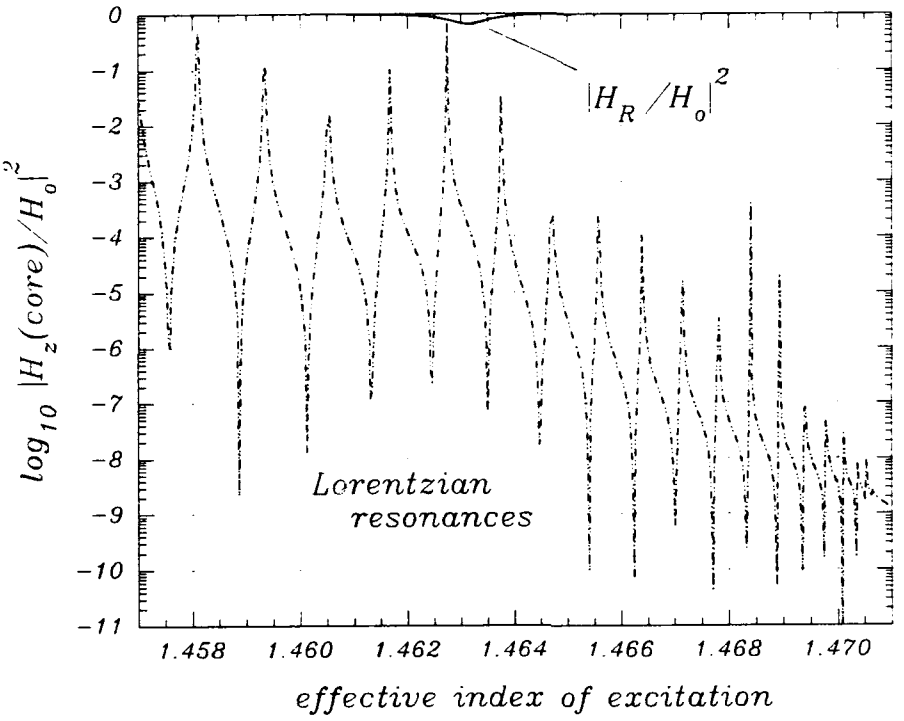

Figure 15: *Normalised magnetic field intensity at the upper edge of a 30 μm multi-mode core, for an oil index of 1.418; for other parameters refer to text*

for the extended range LRSP modes, and then the value of A_0 can be found simply by scaling the $L(n_{eff})$ function to fit the calculated $H_z(n_{eff})$ function. The absorption parameter controls the narrowness of the line; 2α equals the FWHM (in effective index) of the resonance. For incidence of a laser beam at the centre of a resonance, more efficient coupling into the associated core mode will occur if the angular linewidth of the Lorentzian exceeds or roughly equals the angular bandwidth of the laser beam. The strength of the resonance also scales with the value of A_0, which is itself related to the geometry and parameters of the MFSPR structure. For good mode selection, two criteria must be fulfilled. Firstly, A_0 must peak strongly at the effective index corresponding to excitation of the desired mode (dropping off sharply for adjacent modes), and secondly the Lorentzian linewidth must be sufficiently broad to allow efficient excitation of the core mode from a laser beam. In Figures 16 and 17, the parameters are plotted against effective index, with oil indices of 1.418 (Figure 16) and 1.4285 (Figure 17). $H_z(n_{eff})$ is the field at the upper edge of the core; it can in turn be related to the power in the guided mode. Higher order modes have stronger interface fields (they are less well confined) than lower order modes. The modal power plots takes care of this effect, normalising the modal

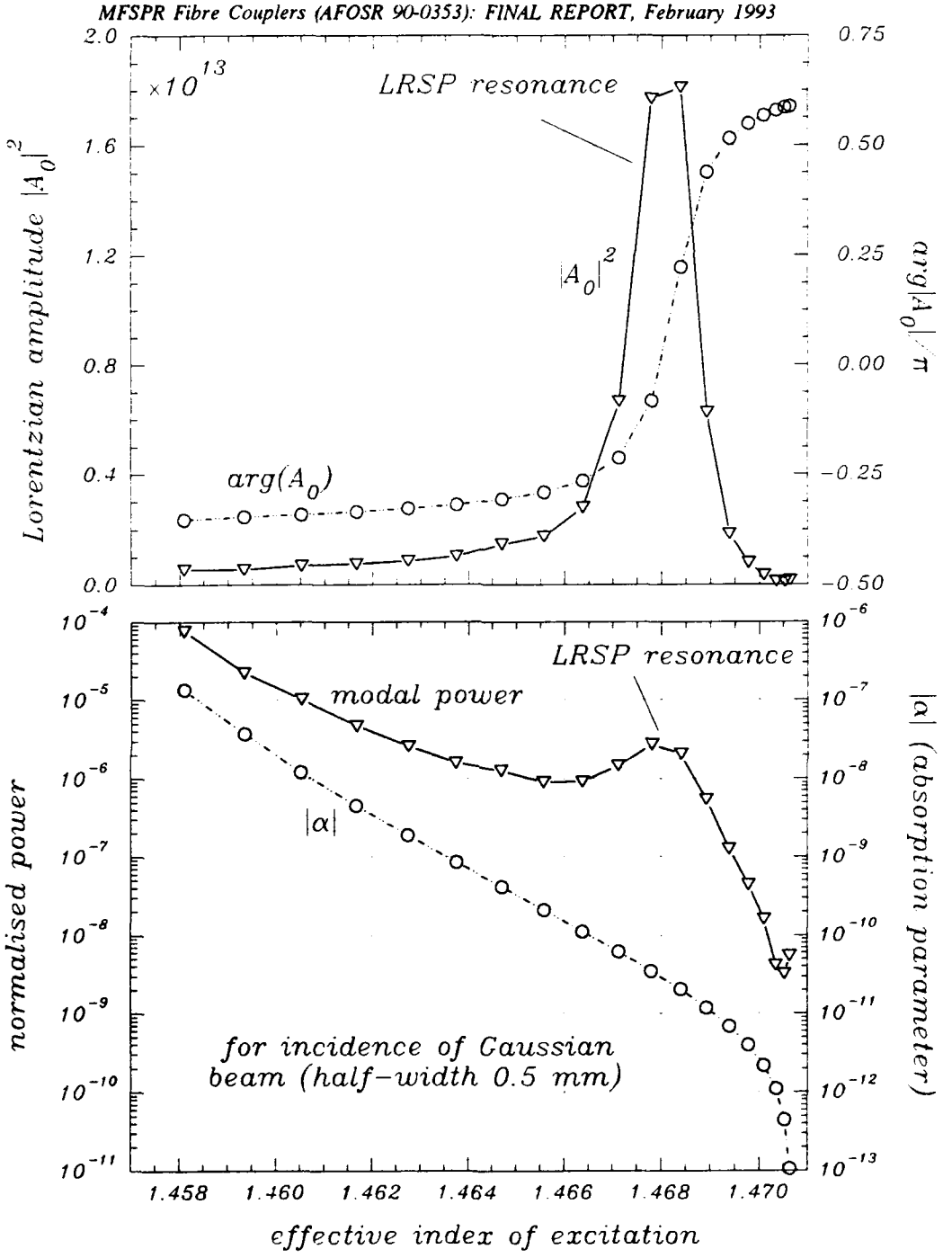

Figure 16: Lorentz parameters for a 19-mode MFSPR coupler with a LRSP resonance at an effective index of 1.468; each data point corresponds to one mode; the metal is silver (26 nm thick), the wavelength 633 nm, the oil thickness 1000 nm, the cladding thickness 4 μm, the core width 30 μm, and their respective indices are 1.4285, 1.457 and 1.47066. The silver dielectric constant is $-17.7-j0.717$ and the prism index 1.8; note the poor mode power selectivity.

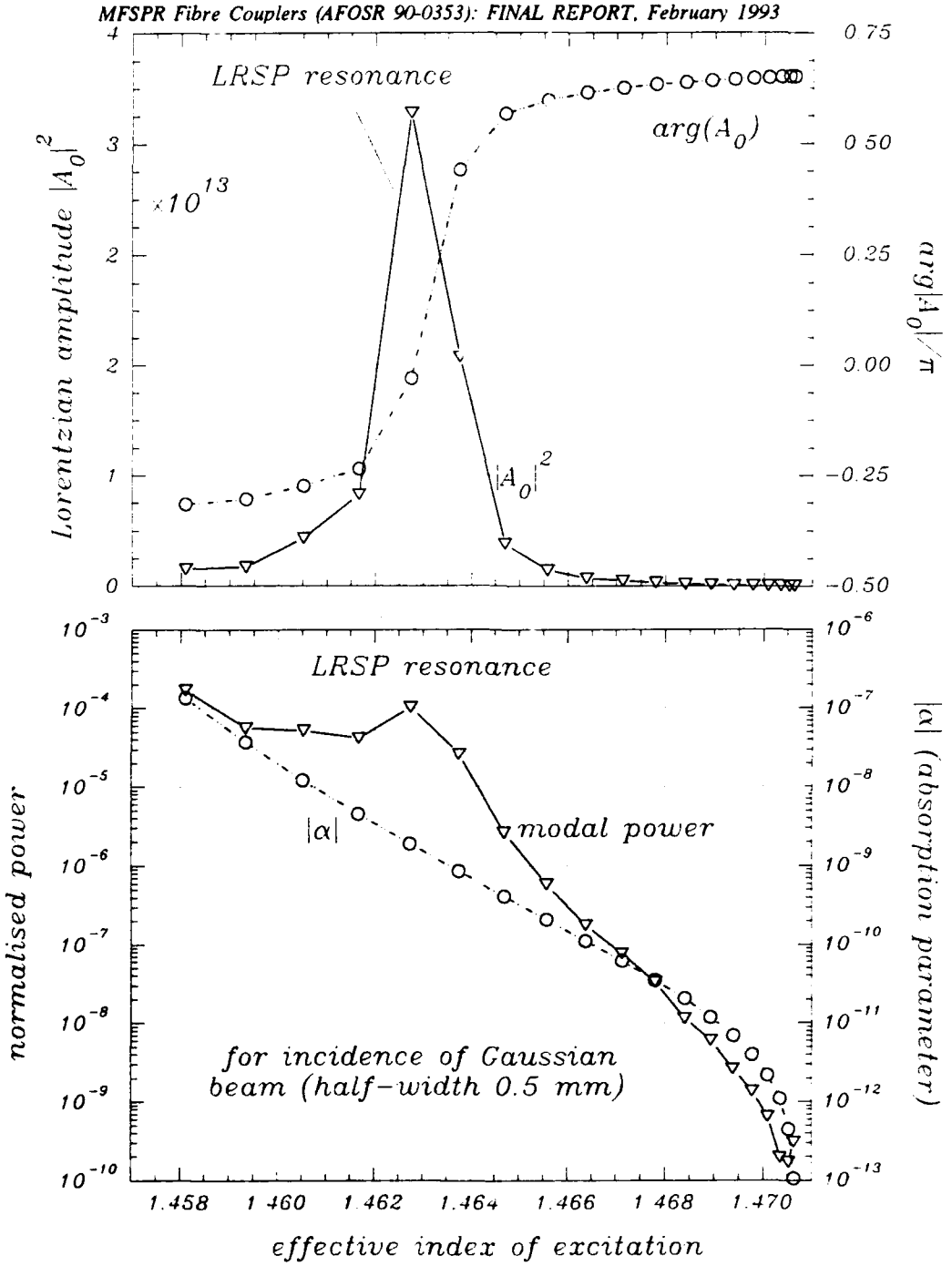

Figure 17: Lorentz parameters for a 19-mode MFSPR coupler with a LRSP resonance at an effective index of 1.462; each data point corresponds to one mode; the metal is silver (26 nm thick), the wavelength 633 nm, the oil thickness 1000 nm, the cladding thickness 4 μm, the core width 30 μm, and their respective indices are 1.418, 1.457 and 1.47066. The silver dielectric constant is −17.7−j0.717 and the prism index 1.8; note the poor mode power selectivity.

Table I

Lorentzian resonance parameters: Dual-mode case

oil index	1.4285		1.4180	
mode type	LP_{01}	LP_{11}	LP_{01}	LP_{11}
$\|A_0\|$	7.8	58	51	9.1
α	3.9×10^{-5}	3.1×10^{-6}	4.1×10^{-7}	5.9×10^{-5}
n_R	1.4683	1.4619	1.4683	1.4617
n_R-n_{0m}	2.5×10^{-6}	-6.9×10^{-5}	2.3×10^{-6}	-2.0×10^{-4}

power to the total incident power in a Gaussian beam of half-width 0.5 mm. It may be seen that, whereas the second criterion (above) is well fulfilled, the first is by no means satisfied; only a slight increase in modal power occurs in the vicinity of the LRSP resonance, even though the A_0 parameter peaks quite well. The MFSPR structure performs rather poorly as a mode selector.

3.4.3.2 Excitation through the prism: dual-mode case

Next, excitation of a dual-mode fibre MFSPR structure is analysed using this approach. By applying Fourier transform techniques, an elegant mathematical expression for the power in the core as a function of distance and effective index can be reached for incidence (on the base of the prism) of a laser beam of finite angular bandwidth. We start with a Gaussian beam of amplitude profile:

$$g(\zeta) = g_o \exp\{-(\zeta/a)^2/2\} \qquad (8)$$

where ζ is a coordinate normal to the beam direction in the prism. The beam intensity decays to 1/e of its central value at $\zeta=a$. In a procedure which involves the convolution of this Gaussian and a single Lorentzian line, the following closed form solution for the power in the core can be reached [to be submitted for publication]:

$$\frac{H_z(x)}{H_0} = \frac{A_0 \Re(\xi)}{4\sqrt{\pi}} \exp\{-j\beta_o x - (\varsigma x)^2\} \mathrm{werfc}\Big(j(\xi - \varsigma x)\Big)$$

where

$$\xi = k_v(\alpha - j[n - n_{0m}])an_p/n_{0m}, \quad \varsigma = \{n_{0m}/(an_p\sqrt{2}\} \tag{9}$$

and the function werfc is the "w" error function

In order to find the optimal parameters, the $x-$dependence of the layer was explored for a dual-mode device. The best performance was found with prism, cladding and core indices of 1.8, 1.457 and 1.47066; oil, metal, cladding and core thicknesses of 1 μm, 26 nm, 2 μm and 2.8 μm; and a silver film ($\epsilon_m = -17.7 - j0.717$ at the operating wavelength of 633 nm). The results for this case are plotted in Figure 18, with oil indices of 1.4285 and 1.418, matching to the LP_{01} and LP_{11} modes respectively. The related Lorentz parameters are tabulated in Table I. The Gaussian input beam is taken to have a FWHM width of 1 mm in the prism. It may be seen that in both cases, the best modal discrimination occurs at z=0.8 mm. Although the result is quite encouraging – the unwanted mode in each case is moderately suppressed at this point – one must bear in mind that prism in-coupling is not analogous to excitation from the fibre; indeed (see next section), the modal selection is much less good in that case. Next, the power in each mode at z=0.8 mm is plotted (Figures 19 and 20) against the effective excitation index, i.e., the index along the prism base of the plane wave at the centre of the Gaussian's angular spectrum; this corresponds to the experimental case reported in section 3.6. The device in Figure 19 was designed (see section 3.5) to match with maximum discrimination to the LP_{01} mode of the core; despite this, a substantial amount of light is coupled into the LP_{11} mode when the effective index of the exciting light matches its mode index. In Figure 20, the device is redesigned for matching the LRSP mode to the LP_{11} mode of the core; this time the discrimination is much better. Notice the accuracy of the design procedure in producing a LRSP resonance (the dip in the reflected light in the figures) that matches well to a given waveguide mode. In summary, the theory shows that an optimised device can provide good discrimination of the LP_{11} mode over the LP_{01} mode, whereas the LP_{01} mode is less well selected at its resonance. This is largely because the higher order mode penetrates much further into the cladding layer, resulting in strong coupling even when the mode match is LRSP/LP_{01}.

3.4.3.3 Excitation from the fibre: dual-mode case

To illustrate this point further, the Poynting vector distributions (proportional to the real part of $\beta|H|^2/\epsilon_n$) of the *normal modes* of a composite dual-mode structure are plotted in Figure 21. Note that $Re\{\epsilon_m\} < 0$ the Poynting vector is negative inside the metal layer; its modulus

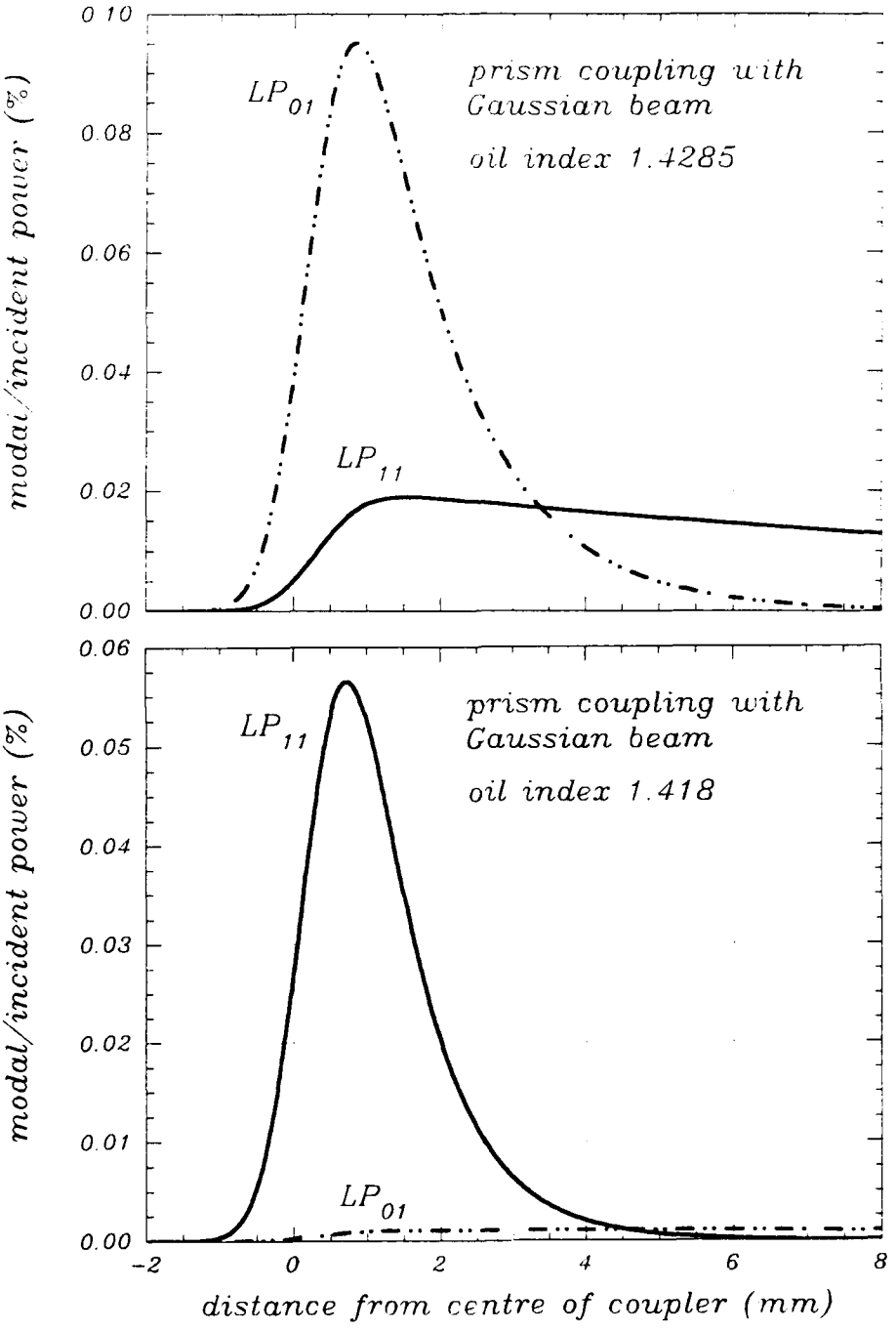

Figure 18: Power coupled into each mode of a dual-mode MFSPR coupler, plotted against distance from the centre of the device for incidence of a Gaussian beam of HWHM a=0.5 mm; the upper and lower cases treat device optimised for LP_{01} and LP_{11} mode selection respectively; note the optimum length for mode selection.

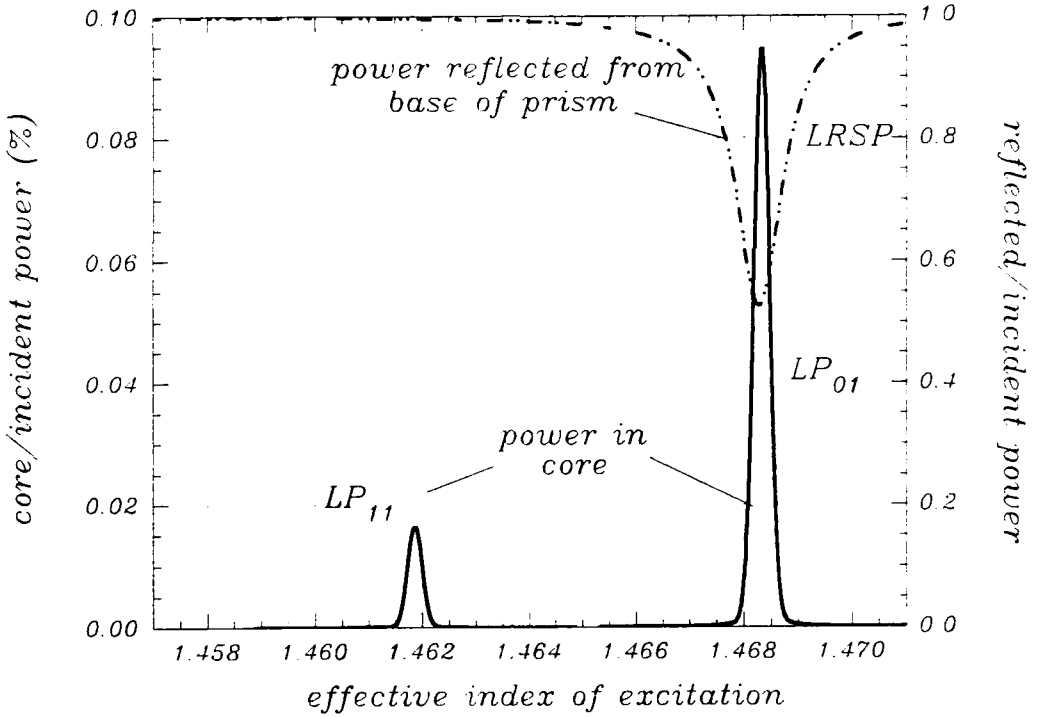

Figure 19: Dual-mode fibre device excited by prism coupling, modelled using the convolution of a Gaussian beam and two Lorentzian resonances. The device was designed for LRSP/LP_{01} matching (oil index 1.4285)

is therefore plotted. Figure 21(a) deals with the case when the LP_{01} mode is matched; two modes appear, one with high and the other with low loss. In general, these modes are both excited for incidence of an LP_{01} mode on an abrupt boundary with the coupler region. If (as is the case in the MFSPR coupler experiments where the core gradually comes up to meet the metal layer) the transition is gentle (i.e., adiabatic), then only the extended range mode will be excited, making analysis of device operation straightforward; and even if this is not so, the high loss mode will be absorbed within a few tens of μm, permitting it to be ignored without affecting the conclusions significantly. The modal discrimination can then be estimated by looking at the shape of the phase-mismatched LRSP/LP_{11} mode; this mode is also plotted in Figure 21(a), and it can be appreciated that a substantial amount of light will be coupled from the LP_{11} mode to the LRSP mode *even when this interaction is strongly dephased*. This result has serious implications for the utility of MFSPR couplers as mode selective taps. As already mentioned, this occurs because of the different penetration rates of the evanescent tails of the LP_{11} and LP_{01} fields in the cladding. Next, the modal field distributions for perfect matching between LRSP and LP_{11} modes are plotted (Figure 21(b)). In this case, the modal discrimination is very good – the dephased LP_{01}/LRSP mode has in this case an extremely weak field component in the prism – which is to be expected since

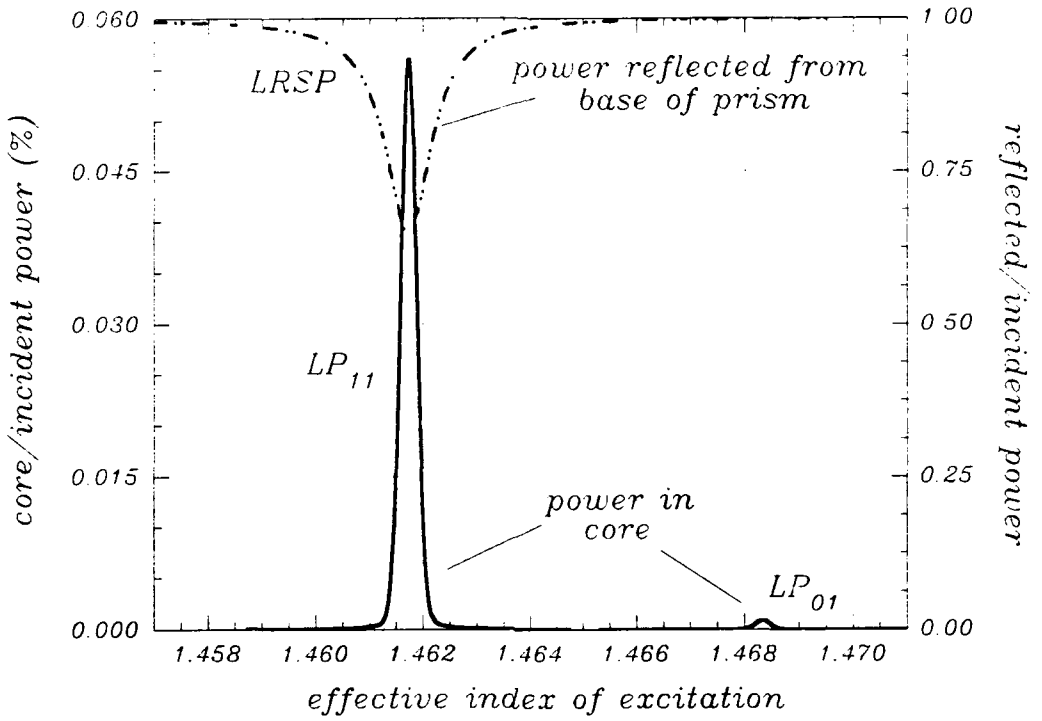

Figure 20: Dual-mode fibre device excited by prism coupling, modelled using the convolution of a Gaussian beam and two Lorentzian resonances. The device was designed for LRSP/LP_{11} matching (oil index 1.418)

the evanescent fields now work in favour of modal discrimination.

3.4.3.4 Excitation from the fibre: multi-mode case

The multi-mode device whose Lorentz parameters were summarised in Figures 16 and 17 will not display good modal discrimination if excited from the core – the same problem arises as in the dual-mode case. Modes with lower values of β will be much more strongly coupled to the LRSP mode than those with higher values. This fact is confirmed in the plots of the Lorentzian amplitudes A_0 for each mode (Figures 16(a) and 17(a)); although these are for the reverse situation of prism-to-guide coupling, they provide just another view of the same problem. Good modal discrimination is acted against by the fact that, for matching to a mode of given order, lower order modes are successfully de-selected, whereas higher order modes tend to be more strongly selected, and therefore cannot be suppressed.

3.4.4 Conclusions

Theoretical modelling shows that operation of MFSPR couplers as mode selective taps is

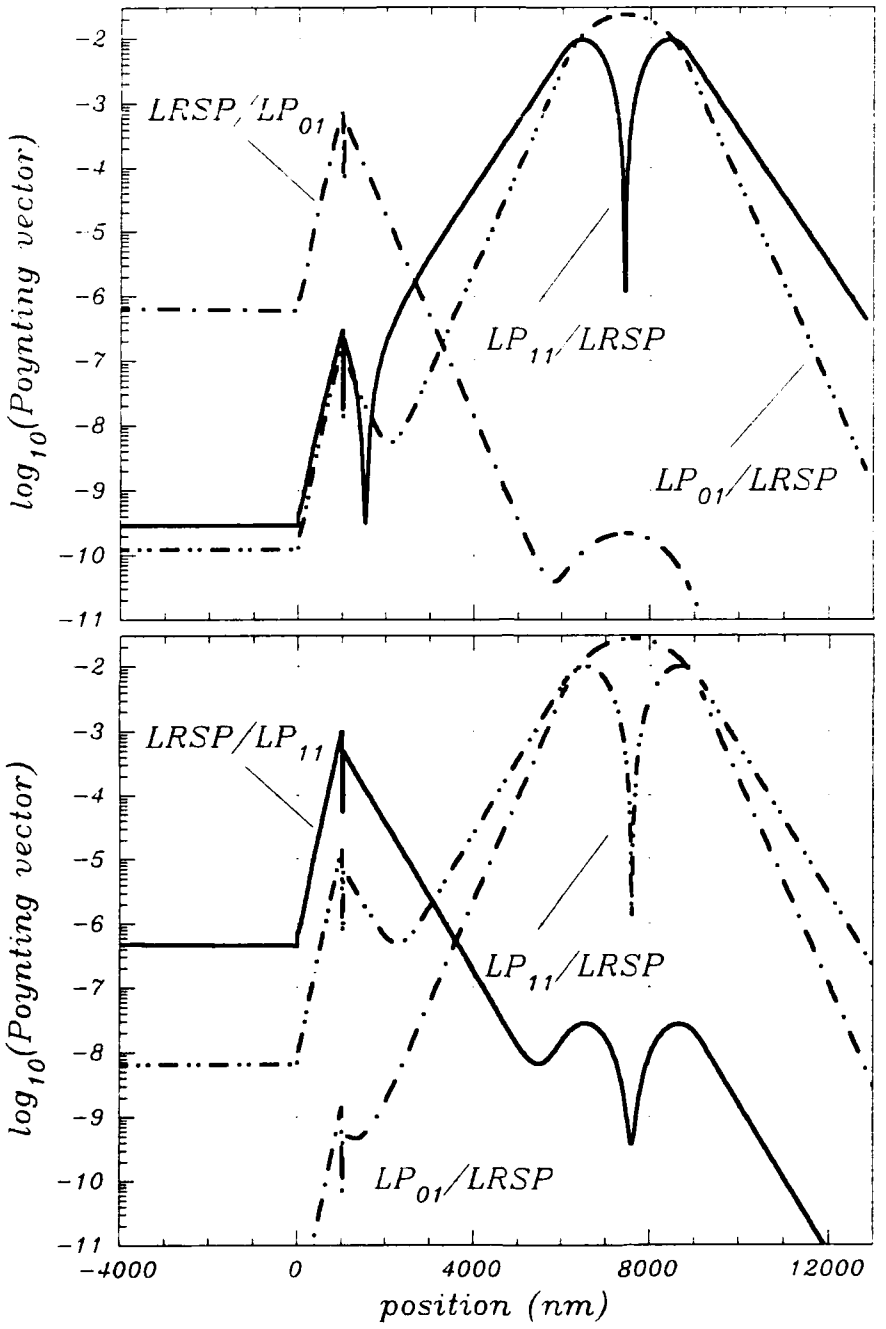

Figure 21: Poynting vector distributions of the normal mode fields for a) LP_{01}/LRSP matching and b) LP_{11}/LRSP matching.

fundamentally limited by the unavoidably stronger coupling that occurs to higher order modes, even when the LRSP resonance matches to the fibre mode to be tapped out. Whether these observations are confirmed in practice will be seen in section 3.6, where a series of experimental results on dual and multi-mode fibres is presented.

3.5 Device design

3.5.1 Summary and objectives

The device design has three main objectives. The first is a modal selectivity or finesse sufficiently high to achieve low cross-talk between the chosen number of channels; the second is to guarantee low insertion loss and only weak output coupling (1%) of the desired channel; and the third is to achieve tunability on a scale of msec.

3.5.2 Choice of parameters for metal layer

This is chosen using the analysis in the previous section. The trade-off is between film robustness (thickness), high finesse (good modal discrimination) low output coupling efficiency (low insertion loss), and the availability of low index liquid crystals or electro-optic polymers (tunability). The design procedure is first to identify a range of suitable film thicknesses and superstrate indices, and then choose a precise value according to the strength of output coupling desired. This depends on the penetration depth of the evanescent tailing field on the upper side of the deposited metal layer and the distance away of the second fibre or prism. The 1/e decay length of the field is controlled by two parameters at fixed wavelength: the superstrate index and the phase index of the guided modes in the fibre. By choosing a lower superstrate index n_3, the interaction strength is increased. A further consideration is the 1/e decay length of the modes guided in the fibre core; this is largest close to cut-off, i.e, for the higher order modes. For the multi-mode fibre supplied to the project, this length is plotted against mode index in Figure 22 for 633 nm and 800 nm. The choice of silver for the initial experiments was made because of its extremely good properties (low absorption) in the wavelength range of interest to the project. Unfortunately silver films tend to deteriorate with time, forming sulphides on contact with the atmosphere [C31]. An attractive alternative is gold, which while having only slightly higher absorption at 800 nm does not degrade with time.

3.5.3 Wavelength dependence of ϵ_m for silver

A parameter important in accurate design of film thickness is the relative dielectric constant ϵ_m of the metal layer. The value of ϵ_m is known to depend on film thickness, deviating more markedly from the bulk value for very thin layers. Since a MFSPR device based on aluminium requires very thin (< 20 nm) layers whose ϵ_m value is unpredictable, and whose absorption is rather high [D11,D12,D13], we chose to carry out our experiments using silver. In the design calculation, tabulated values of $\epsilon_m = (\epsilon_{mr} + j\,\epsilon_{mi})$ against wavelength

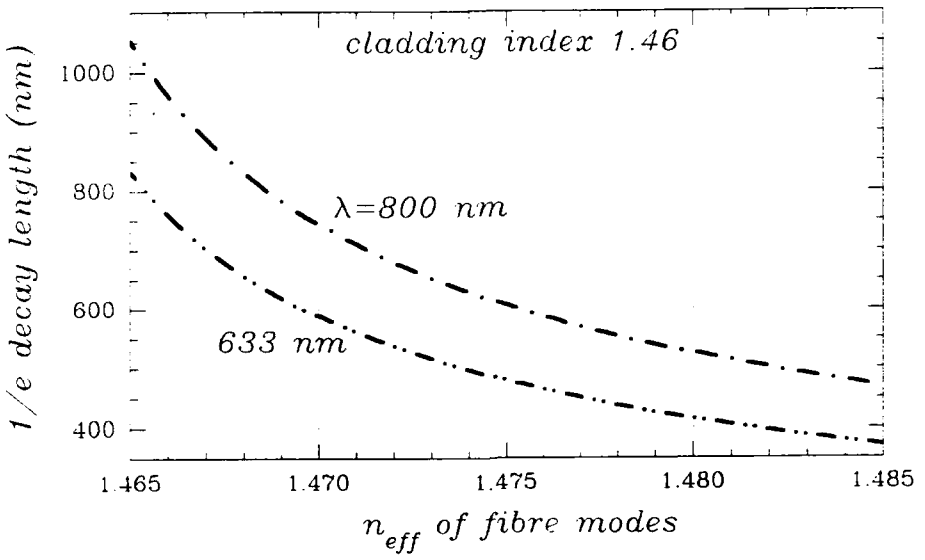

Figure 22 1/e tunnelling depth versus effective phase index of the multi-mode fibre modes for a substrate index of 1.46

were used [E1], and the real and imaginary parts fitted to the polynomials:

$$\begin{aligned} \epsilon_{mr}(\lambda) &= 7.1411 - 0.01177\lambda - 0.00004\lambda^2 - 2.27077 \times 10^{-9}\lambda^3 \\ \epsilon_{mi}(\lambda) &= 0.00133\lambda - 2.5207 \times 10^{-6}\lambda^2 + 1.89937 \times 10^{-9}\lambda^3 \end{aligned} \quad (10)$$

where λ is in nm. These are plotted, together with the experimental data points, in Figure 23.

3.5.4 Signal extraction from LRSP

Prism coupling is not a particularly attractive technique in a practical device, and several other methods exist for extracting the signal from (or coupling it into) the device. One possibility (which could easily be implemented if a practical working device were available) is a second half-coupler block. Another possible technique involves replacing the prism with a fine-pitch refractive index grating. When a LRSP mode is excited, light would then automatically be coupled into free space for detection at a photodiode [D18]. Tunability could still be achieved by using a liquid crystal – with the added advantage that the grating would act as a convenient surface for achieving the desired planar alignment of the liquid crystal.

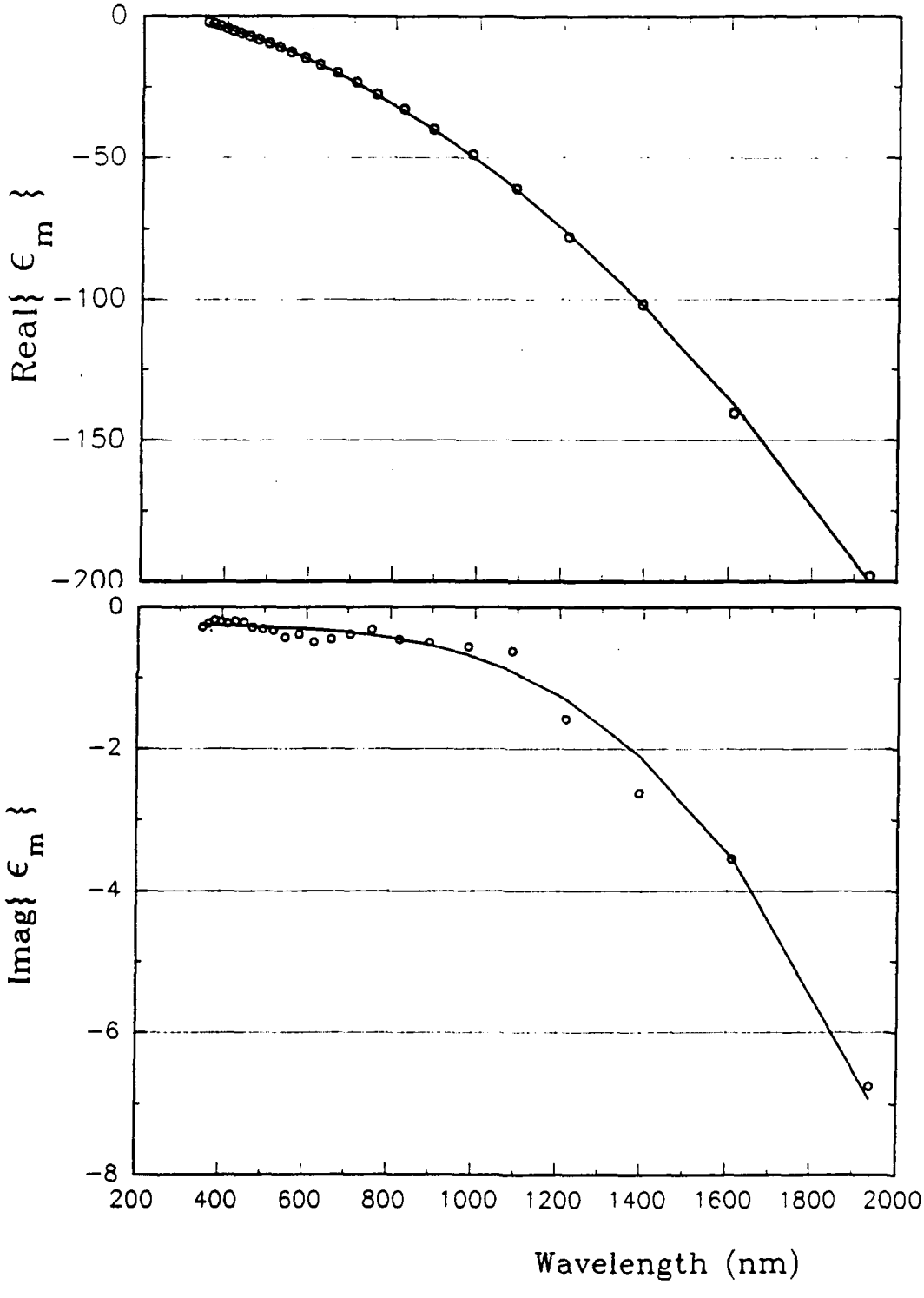

Figure 23 Wavelength dependence of ϵ_m for silver (see text for details) [E1]

3.5.5 Optimisation of the design for best modal discrimination

In spite of the unpromising initial conclusions of the theory section, we used the analysis to optimise the MFSPR structure for the best possible modal discrimination within the known constraints of the device performance. This was achieved by plotting the ratio of the power coupled out into the prism, P_{out}, to the power incident in the core, P_{in} (see configuration in Figure 13). The calculation was carried out by following the behaviour of the LP_{01}/LRSP and LP_{11}/LRSP composite modes as the oil index was varied, and using their field distributions to estimate P_{out}/P_{in} by integrating across the fibre core (at the input face of the MFSPR coupler), and along the prism base. The resulting number is a direct measure of the fraction of the input power in a given mode that gets coupled out into the prism for subsequent detection. Clearly, at an appropriate value of n_{oil}, a good mode-selective tap would couple one mode out to the exclusion of the other, while achieving the reverse at another value of n_{oil}. The best result from extensive calculations is presented in Figure 24, where the LP_{11} modal selectivity $R_{11}/(R_{01}+R_{11})$, where R_{nm} is the coupling ratio for the LP_{nm} mode, is also plotted. This parameter equals 1 when the LP_{11} mode is perfectly selected, and 0 when the LP_{01} mode is perfectly selected. The optimisation procedure involved sifting through the large number of adjustable parameters. The oil, metal, cladding and core dimensions are 1 μm, 26 nm, 5 μm and 3 μm; the prism, cladding and core indices are 1.8, 1.457 and 1.47066; and the oil index is 1.418 for LP_{11} selection and 1.4285 for LP_{01} selection. Equal input power is assumed in the LP_{01} and LP_{11} modes, and the best LP_{01} modal selectivity is $(1-0.35) = 0.65$.

Also plotted (in Figure 25) are the real and imaginary parts of the effective index n_{eff} of the LP_{01}/LRSP and LP_{11}/LRSP composite modes as the oil index is varied. The attenuation (represented by a large negative imaginary part of n_{eff}) peaks at resonance, which accords with the Lorentzian absorption line discussed above in section 3.4.3.1.

3.5.6 Routes to tunability

The ultimate aim of the project was to obtain rapid modal selection between up to 5 channels in the multi-mode fibre supplied to the project, the interchannel cross-talk being less than -20 dB. Several routes to tunability are feasible. The first is heating the oil layer between the surface of the metal and the upper prism base or second polished fibre. This could be achieved by passing a current through the metal layer. The response time in such an arrangement will be limited by the cooling rate after switching off the current. Although we have not analyzed this in detail, we expect the recovery times to be of order 50 μsec, which would allow interchannel switching at msec rates. The coefficient of index change with temperature is around -3.8×10^{-4} per degree K, so for a range of 0.02 (needed for tuning over the multi-mode fibre modal spectrum) the temperature would have to vary from ambient to around 70°C. The response time could be improved by incorporating a Peltier cooler below the fibre, perhaps replacing the glass fibre mounting blocks with a thin glass substrate.

The second is to choose a liquid crystal with an ordinary index below that of silica, and

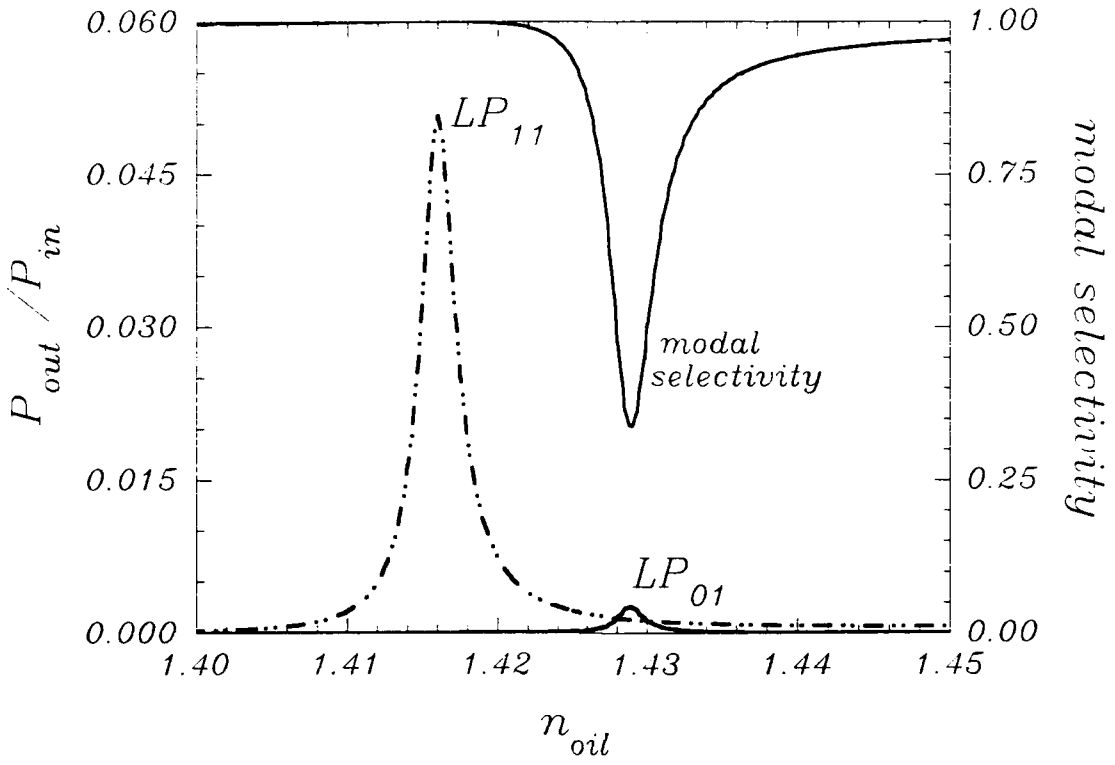

Figure 24: Mode selectivity in optimised dual-mode fibre device; the actual theoretically predicted power leaving the prism is normalised to the power entering the device from the fibre (see Figure 13), for phase matching to the LP_{01} and LP_{11} modes.

arrange it in a liquid crystal cell in planar alignment, the axes of the molecules lying along the fibre axis. Applying a voltage to the cell will cause the molecules to turn towards to surface normal, resulting in an increase in the refractive index experienced by the LRSP mode and thus tuning the device. The most critical aspect of this solution is the availability of a suitable liquid crystal – not many crystals have a sufficiently low ordinary refractive index. Switching times of order a msec are feasible.

The third route involves using an electro-optic polymer, which is either spin-coated directly onto the metal layer or onto the polished fibre before deposition of the metal. We approached Prof Paras Prasad of SUNY at Buffalo about the refractive index, electro-optic coefficients and availability of these materials, but he was not able to help us materially.

In view of the negative results on modal selectivity, we have not pursued the tuning options, concentrating instead on trying to improve the selectivity since without this the MFSPR mode selective coupler will not work.

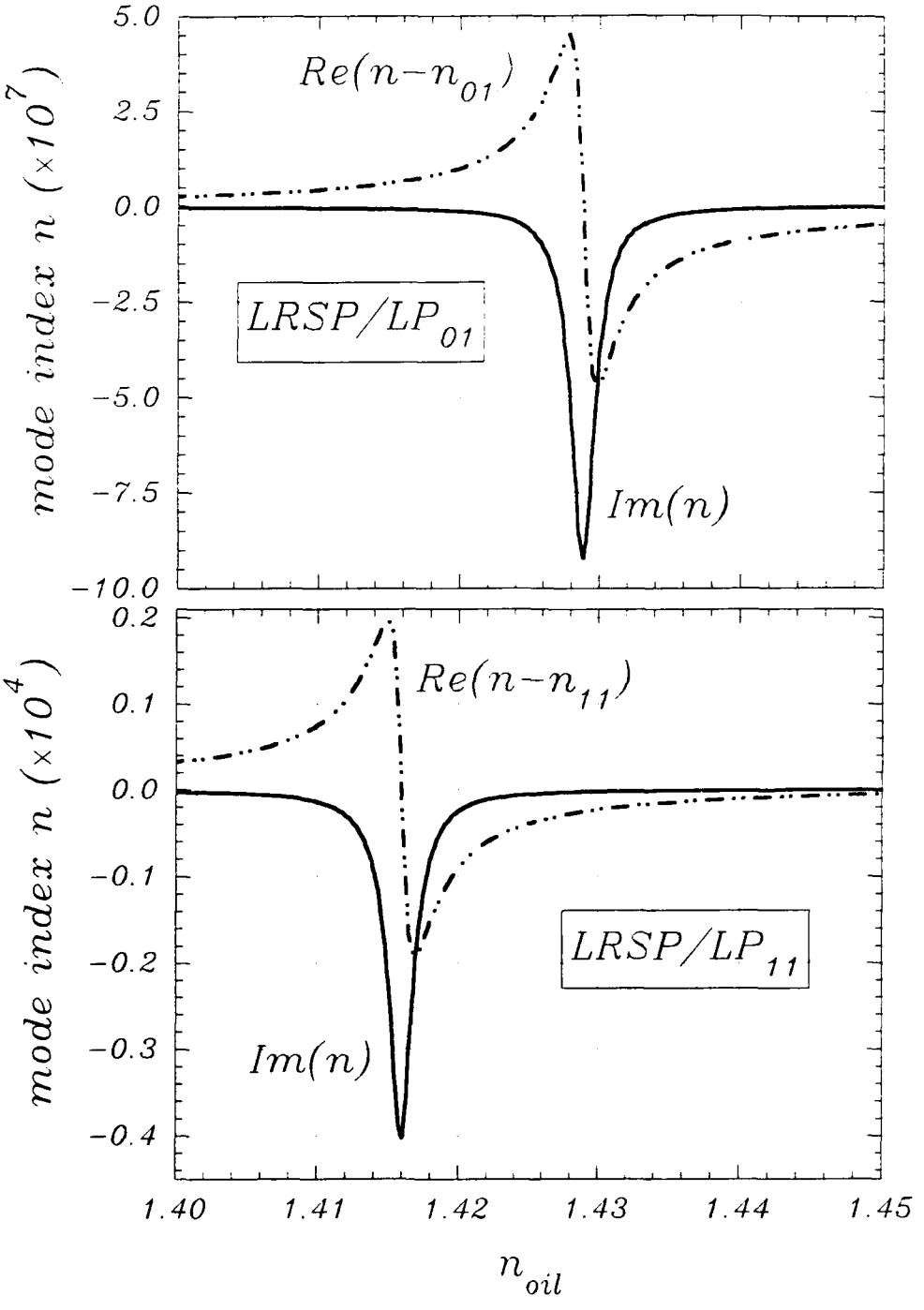

Figure 25: Real and imaginary parts of refractive index for the extended range LRSP modes when matched a) to the LP_{01} mode and b) to the LP_{11} mode.

3.6 Experimental results

3.6.1 Summary

Altogether, 4 single-mode, 10 dual-mode and 6 multi-mode side-polished coupler blocks were prepared. From these, a range of metal-coated MFSPR devices were made (see Table II), sometimes by re-using an existing coupler block. In this section, the main experimental results on these devices are described. In section 3.6.2 the roles of interaction length (controlled by the radius of curvature in the block) and polishing depth (controlled by

Table II

Couplers fabricated during project					
Single-mode couplers		*Dual-mode couplers*		*Multi-mode couplers*	
4		10		6	
Ag	Al	Ag	Al	Ag	Al
0	1	4	1	4	1

polishing time) are discussed. Next, the behaviour of a dual-mode device optimised for best modal discrimination is reported. Results on a multi-mode coupler are reported in section 3.6.4, and conclusions in 3.6.5.

3.6.2 Effects of different interaction lengths and polishing depths

These were studied with a view to optimising the device performance, in spite of the less than promising conclusions from the modelling. It was clear that if the interaction between the fibre mode and the LRSP is strong, then a high degree of attenuation would occur, and too much light would be coupled out in one device. A more subtle effect is the broadening in the sharpness of the resonance that is an inevitable consequence of higher coupling levels; this would have the effect of reducing the modal selectivity. When the cladding thickness is reduced to a small value, the Lorentzian line-widths broaden out owing to the greatly increased coupling strength. Fibre modes are then strongly excited independently of the LRSP resonance, simply because the fields are able to penetrate the metal layer and couple into the core regardless of the presence or absence of a true LRSP mode.

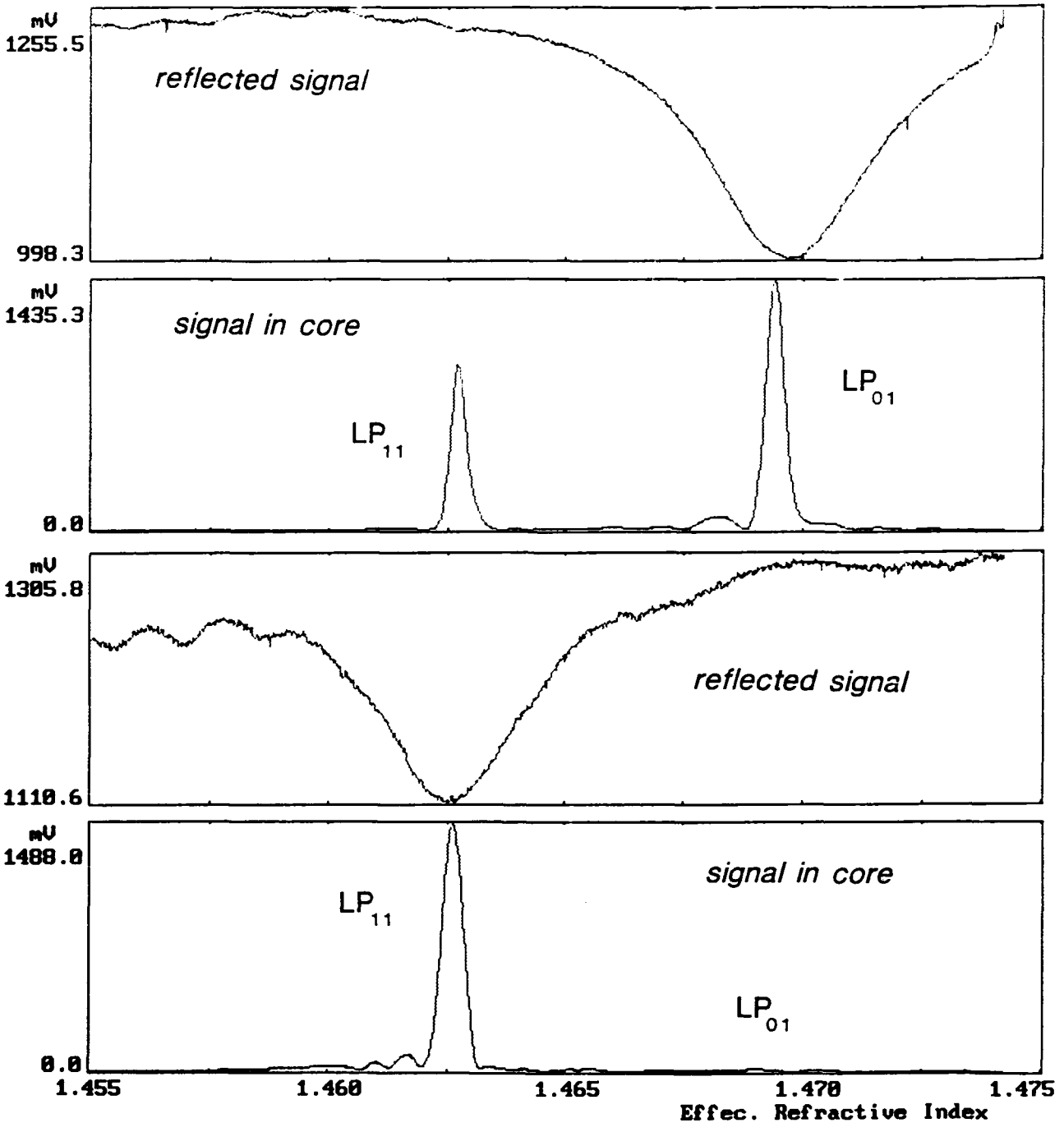

Figure 26: Experimental prism coupling to the LP_{01} and LP_{11} for two different values of oil index, matching the LRSP mode to the LP_{01} and LP_{11} modes respectively. The discrimination agrees well with the numerical simulation (Figures 18 to 20).

3.6.3 Dual-mode fibre devices

Results on the modal selectivity of an optimised dual-mode fibre device (following the design procedure described in Section 3.5) are presented in Figure 26. The device was formed from a side-polished dual-mode fibre coated with 26 nm of silver and tested at 632.8 nm with a He-Ne laser. Measurements were carried out for two different oils, one with index 1.418, and the other with index 1.4285, providing matching for the LRSP/LP_{01} and LRSP/LP_{11} interactions (effective phase indices 1.4693 and 1.4627 respectively). The modal selectivity was investigated by measuring the power in the fibre core as a function of prism in-coupling angle, the peaks (which occur when the fibre modes are phase-matched to the field at the base of the prism) being used to assess the efficiency of coupling to each mode. Next, we defined a normalized parameter $D = P_{11}/(P_{01}+P_{11})$, which is a measure of the modal discrimination; when D approaches unity, the LP_{01} mode (power P_{01}) is strongly excited and the LP_{11} mode (power P_{11}) is not, and when D is zero the reverse is true. Referring to Figure 26 – when the LP_{01} mode is matched to the LRSP mode, the best modal discrimination D achieved in the device is 0.4, and when the LP_{11} mode is matched, it is 0.98. In each case, the dip in the reflected light, which corresponds to the LRSP resonance, coincides as designed with the LP_{01} or LP_{11} mode. The theoretical prediction in Figure 19 for the value of D in the case of matching to the LP_{01} mode is somewhat better, agreeing quite well with the experimental value. The amount of light coupled in when the polarization state is rotated by 90° (TE excitation) is 30 dB less, which represents very good TE suppression. We have also investigated temperature tuning to characterize the effects of different superstrate indices; a combination of heater and Peltier cooler were used to control the temperature. Although promising, the results of this study were very preliminary and were not pursued owing to time constraints; they are not be reported here.

In summary, the experiments on an optimised dual-mode fibre device have shown a strong LRSP resonance with modal selectivity that agrees with the theory, tunability being achieved by varying the superstrate refractive index. The coupling efficiency for TE polarization was ~30 dB below the TM.

3.6.4 Multi-mode fibre devices

The results of prism coupling experiments on several different multi-mode fibre devices are now presented. Two devices were tested, with code numbers D5D (polishing depth ~500 nm from the core, silver film 24±3 nm) and D7B (polishing depth 2.5 μm, silver film 26±6 nm). The approximate geometry of a side-polished multi-mode fibre block is sketched to scale in Figure 27. The Corning fibre has a depressed cladding ring, with an index of 1.450, a core of index 1.4675 and a cladding index of 1.4536. Some uncertainty exists as to whether, in the polishing process, the core was broken into, particularly for device D5D. This is a difficult issue to resolve in practice, since the overlap between the polished surface and the large core mode is very small (200× smaller than in the dual-mode case). Such a

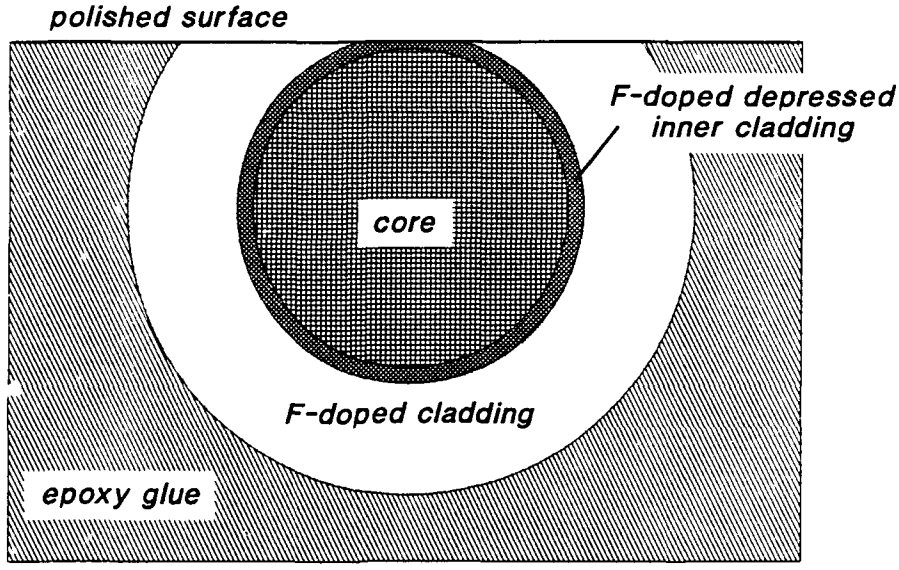

Figure 27: Sketch (approximately to scale) of multi-mode side-polished fibre cross-section. The core diameter is 50 μm, the depressed cladding ring 5 μm wide, and the main cladding 32.5 μm thick. The indices are 1.4675, 1.450 and 1.4536 respectively.

weak interaction means that, even if the core was touched, a drop of oil whose index just exceeds the core index might not strip away very much of the light. The general features predicted by the theory are clearly present – the higher order modes are more strongly coupled than the lower orders, with some enhancement in the coupling to modes that lie underneath the LRSP resonance.

One feature of the multi-mode measurements was that they changed significantly with time, perhaps because the oil layer thinned out under constant pressure in the prism coupling rig. Plots of the behaviour in new and aged devices are presented in Figures 29-31. An anomalous and strong peak appears (this was highly reproducible) in the power coupled into the fibre at the lower-order end of the fibre mode spectrum. Also in aged devices, a second dip develops at high values of n_{eff} in the reflected spectrum, which may be attributed to a LRSP mode forming on the polished-away core itself. To confirm the correct functioning of the apparatus, the TE (*p*-polarised) case was investigated (Figure 28), showing a very weak version of the modal spectrum measured in Figure 7. There may also be much more complicated phenomena caused by the fact that rays oblique to the fibre axis can excite fibre modes with skew-rays (whistling gallery modes); this might be important since the prism coupling experiment is performed with a focused laser beam. In summary, although some as yet unexplained features exist in the measured data, the general conclusion as regards the contract is that mode selective taps based on tunable LRSP resonances are not feasible in multi-mode fibre structures.

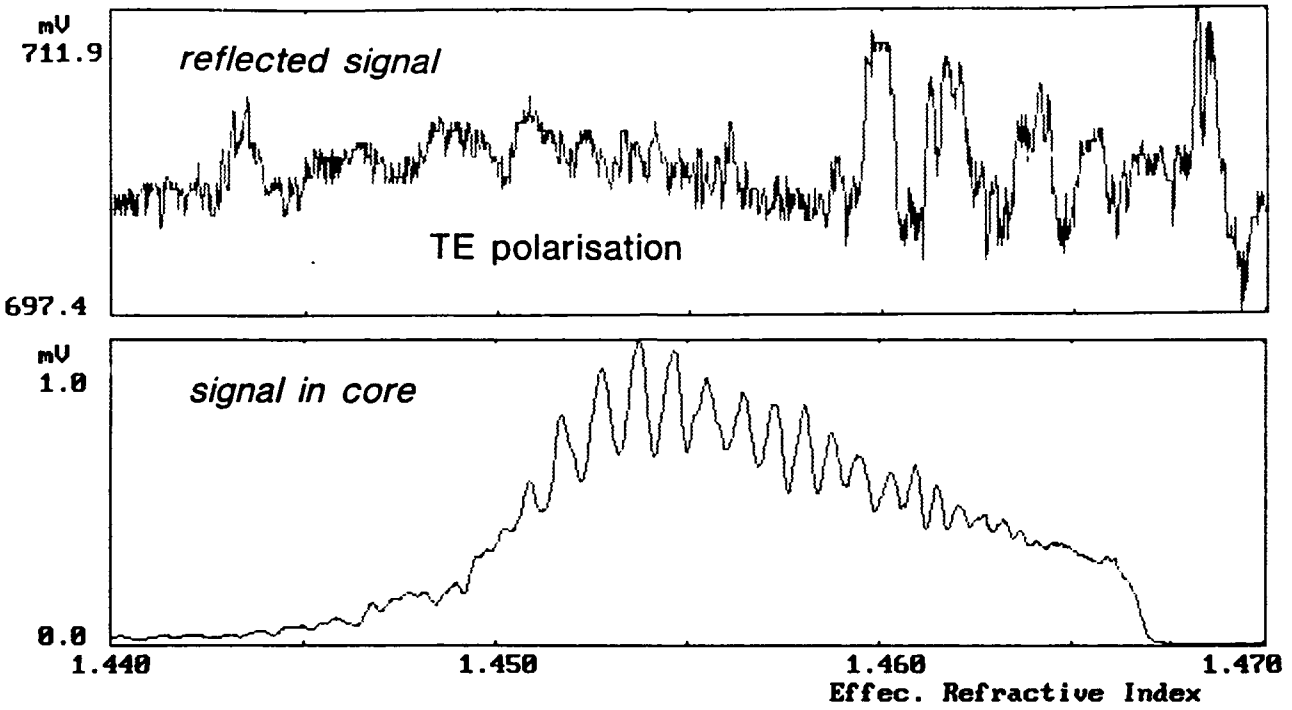

Figure 28: Result of prism coupling experiment on coated multi-mode fibre for TE polarisation. The behaviour closely resembles that observed in an un-coated device (Figure 7), with a much lower signal level. No LRSP resonances exist, and the metal layer acts as an effective barrier.

4. OVERALL PROJECT CONCLUSIONS

Extensive theoretical and experimental modelling of MFSPR couplers in both dual and multi-mode fibres has led to a good physical understanding of the underlying phenomena. Good agreement has been achieved between theory and experiment in nearly all cases. The extended range normal mode (a low loss superposition of LRSP and fibre mode) is the one that participates in the functioning of the device, and these modes have an associated sharp absorption line of Lorentzian shape. The convolution of these Lorentzians with the field of an incident laser beam, incident on the base of a coupling prism, gives a complete picture of the behaviour of the devices for excitation from a prism coupler. In prism coupling, the length dependence of the power coupled into the LP_{01} and LP_{11} modes of a dual-mode

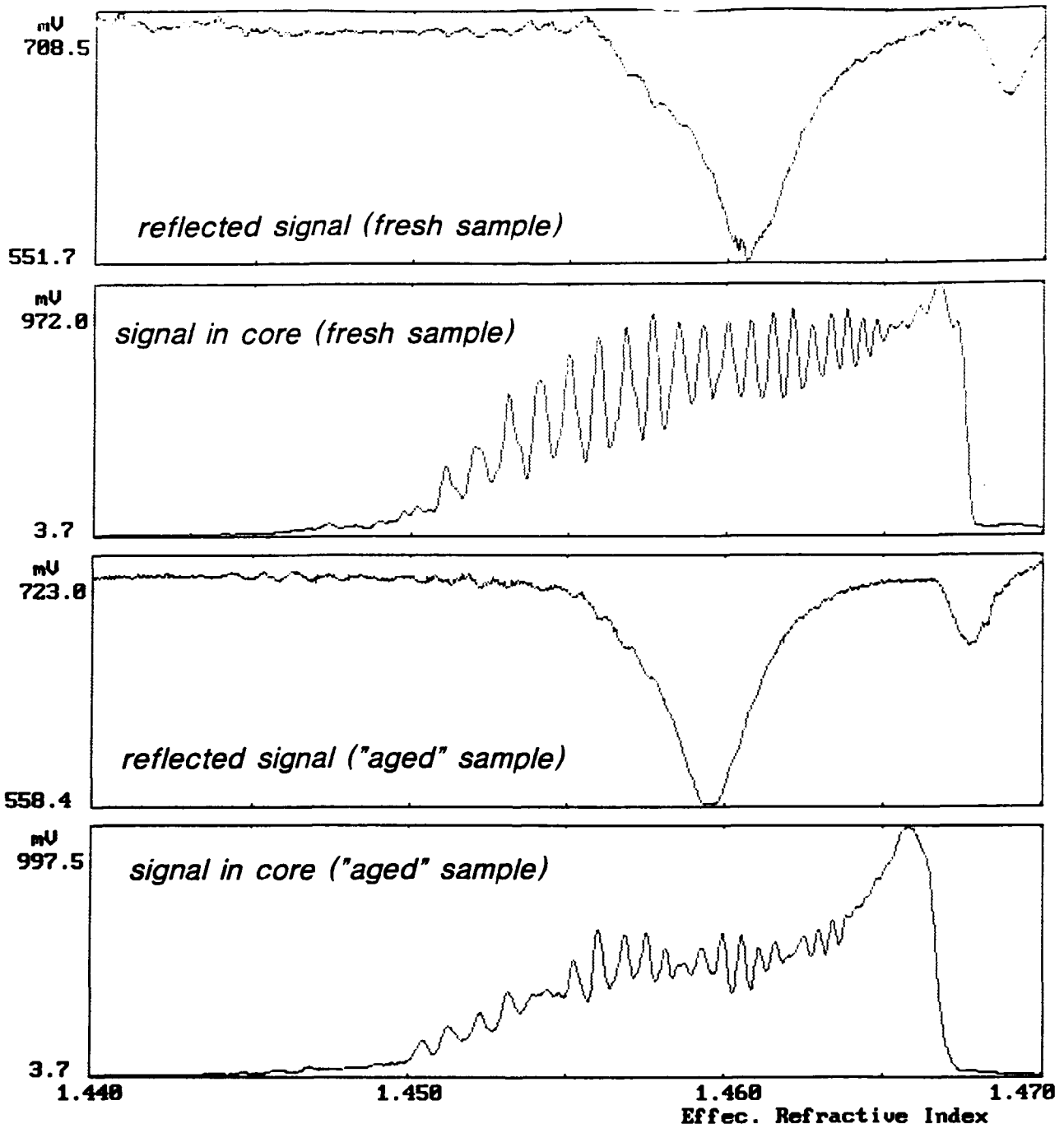

Figure 29: Prism coupling measurements on new and "aged" multi-mode fibre block (sample D7B) with an oil index of 1.418; silver thickness 26±6 nm at 633 nm.

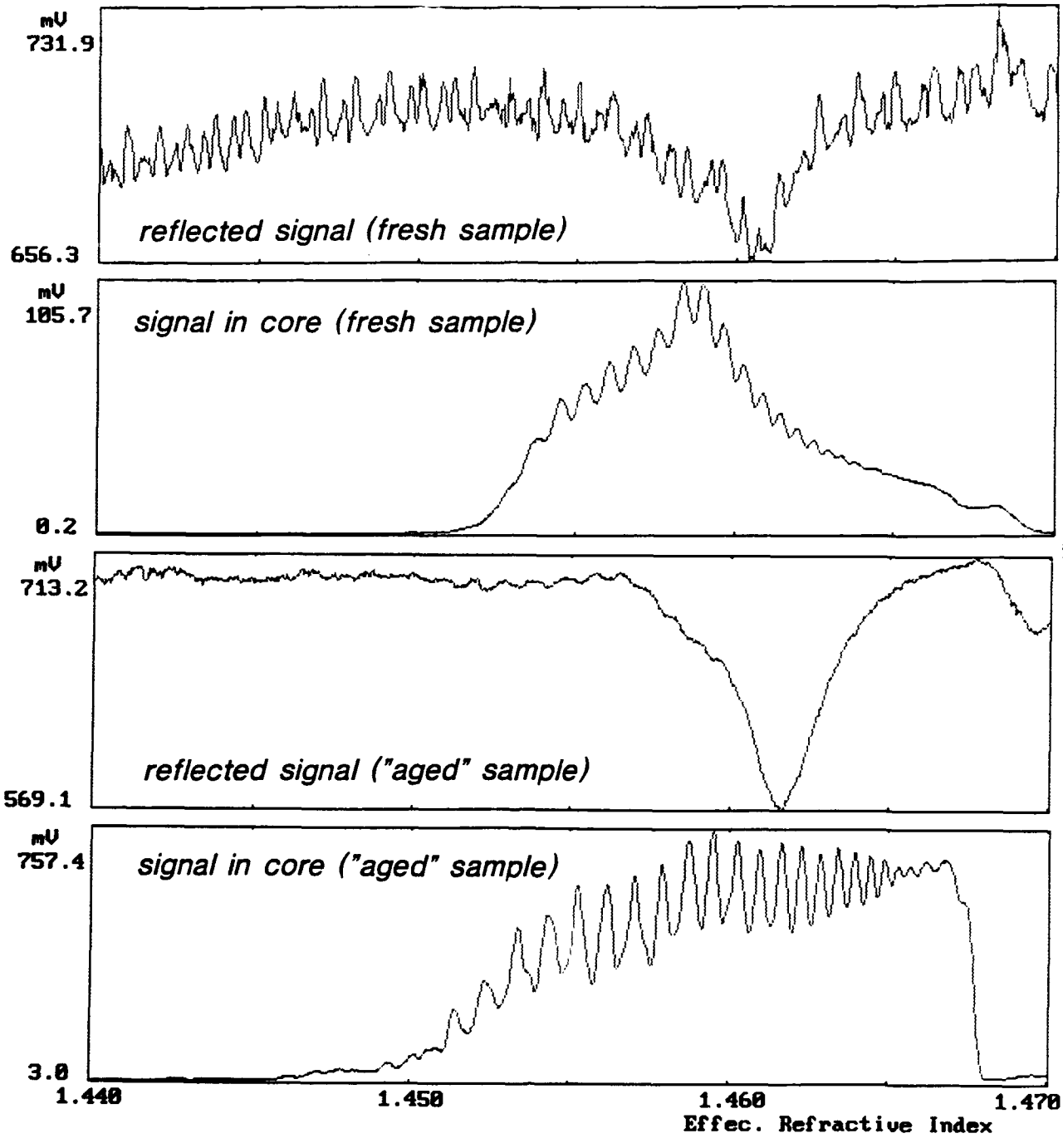

Figure 30: Prism coupling measurements on new and "aged" multi-mode fibre block (sample D7B) with an oil index of 1.420; silver thickness 26±6 nm at 633 nm.

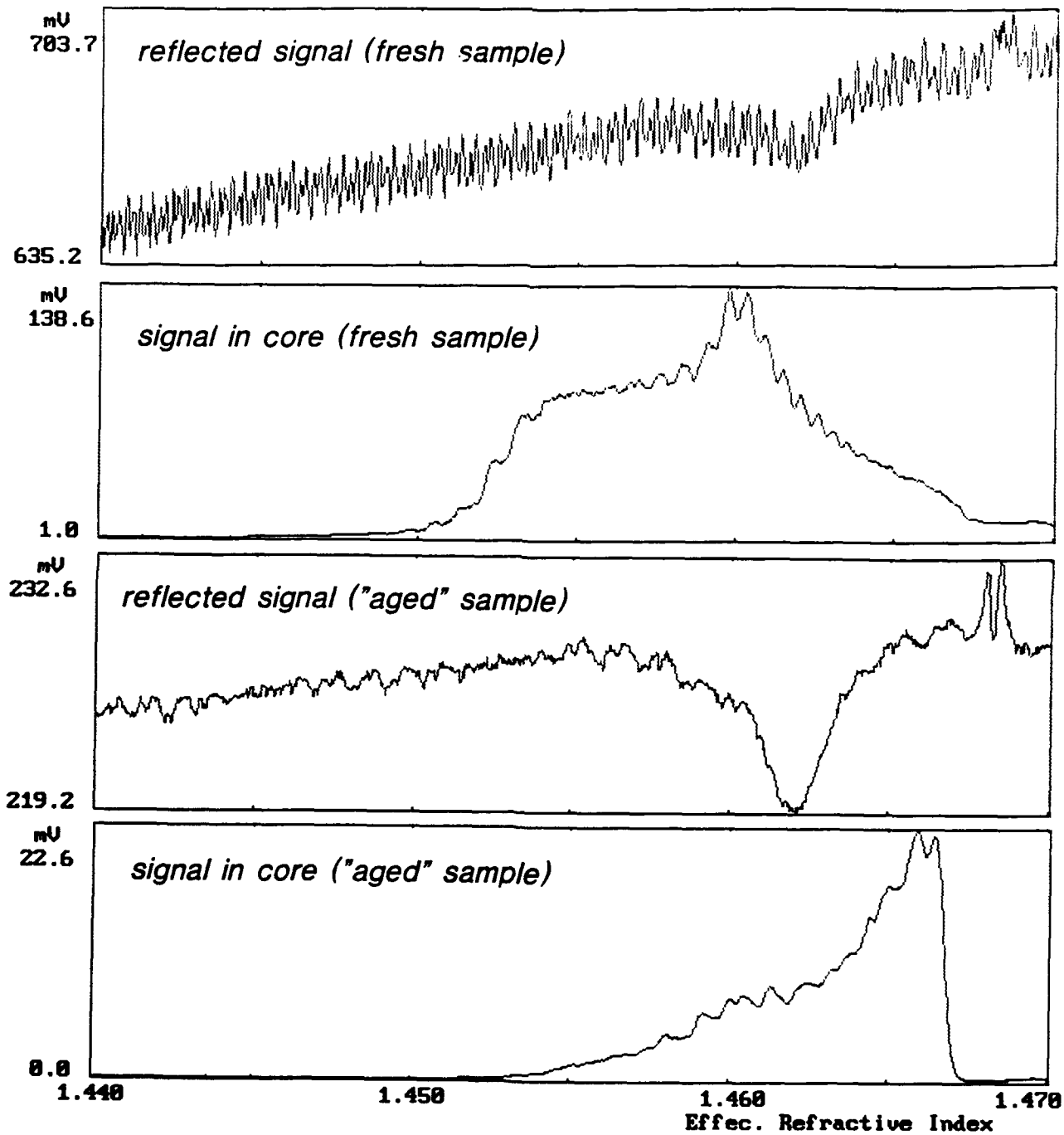

Figure 31: Prism coupling measurements on new and "aged" multi-mode fibre block (sample D5D) with an oil index of 1.422; silver thickness 24±3 nm at 633 nm.

MFSPR coupler is strong, and by appropriate choice of device length, good selective excitation of individual modes of a dual-mode fibre is possible. In our simulation, a coupling length of 0.8 mm was optimal for a Gaussian beam of 0.5 mm half-width. This fair mode selectivity is, however, related purely to the spatial characteristics of prism in-coupling, and does not mean that good modal selectivity is attainable for excitation from the fibre core. In that case, although the resonances are themselves sharp enough to permit good mode selection, their strength of excitation is a very strong function of effective index, owing to the fact that the penetration depth of the evanescent modal fields is a strong nonlinear function of mode order, tending to infinity for a higher order mode at cut-off (i.e., at the core/cladding critical angle). This means that higher order modes can be orders of magnitude more strongly coupled than lower, so that even if a lower order LRSP/fibre mode resonance is excited, significant non-resonant coupling can occur to higher order fibre modes, ruining the mode selectivity of the MFSPR device. If some means of cancelling this effect could be found, i.e., arranging that the tail of an evanescent field lengthens as β falls, then good mode selection might be possible. At present this seems to be a fundamental barrier to the straightforward operation of MFSPR mode selectors. Most of our results are at 633 nm; the performance at 830 nm is expected to be even less good; and the use of a broad-band LED would have a further deleterious effect on device performance.

One interesting solution, which goes part of the way to solving the problem, runs as follows. If a multi-channel communications system could be constructed in which the amount of power coupled into various parts of the mode spectrum is *pre-designed* to compensate for the differing degrees of output coupling at the MFSPR tap, then reasonable mode discrimination might be possible. For example, if the power in the LP_{01} mode (for the situation treated in Figure 24) is increased by a factor of 20, the modal selectivity looks excellent – see Figure 32. Whether this is a viable solution or not could form part of a future research project. The multi-mode problem might also be side-stepped by arranging that the modal power is weaker at the higher order end than at the lower order end. A disadvantage of this approach is that the higher order modes, even if they could be selected out, will be depleted much more rapidly than the lower order modes over a line of receiving stations. A strong signal injected into the fundamental mode would decay at a much slower rate than a weak signal injected into a higher order mode where the coupling is stronger.

The goals of tunability and high performance were not pursued since insufficient modal discrimination was available to make this effort worthwhile. Other LRSP-based devices, such as single-mode fibre polarisers, polarising beam-splitters, and higher-order mode strippers seem to suit the peculiar physical characteristics of MFSPR couplers much better. An alternative channel tapping device could be constructed from a weak grating, written directly in the core by the new technique of UV holography through the cladding glass. This could be constructed so as to tap off, very weakly, all channels at once. The grating couples each channel in a highly precise direction, permitting it to be focused to an individual detector on a photodiode array.

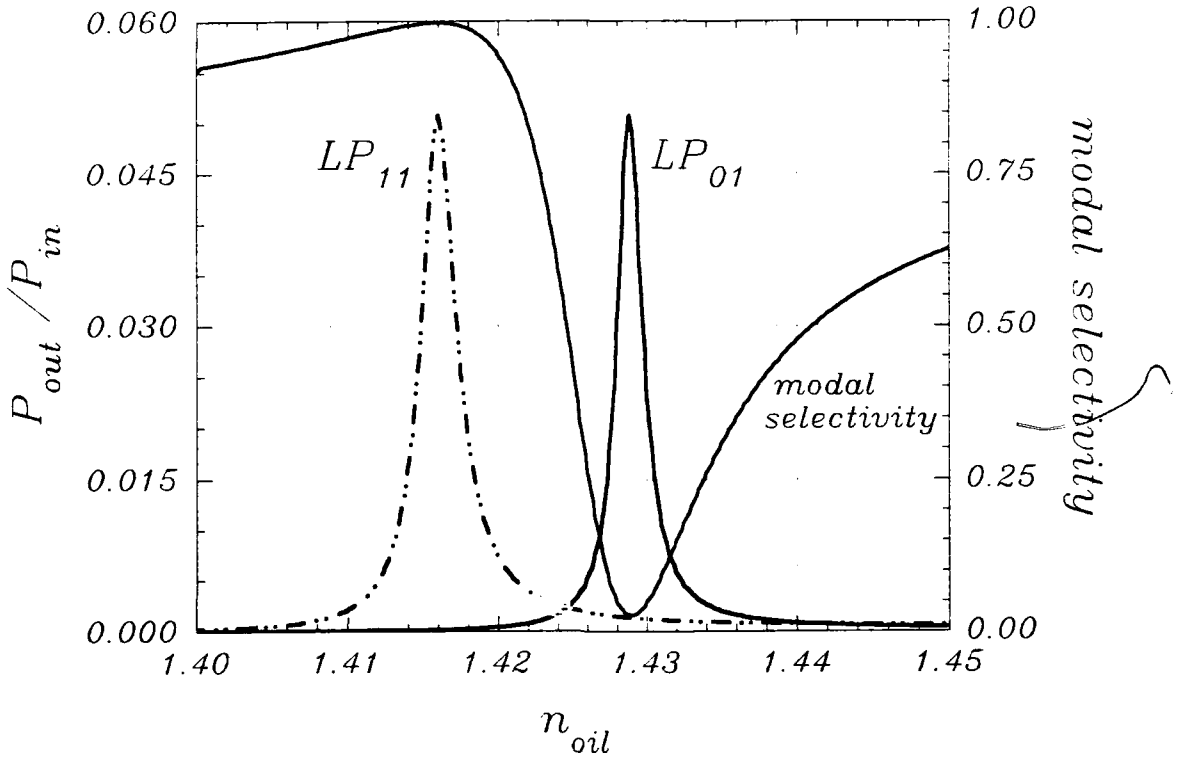

Figure 32: Modal selectivity in Figure 24 when the power in the LP_{01} mode is 20 times stronger than in the LP_{11} mode. The selectivity is quite good.

5. BIBLIOGRAPHIC SURVEY

A. Some Tutorial Papers:

A1 Raether H, "Surface Plasma Oscillations and Their Applications", Phys. of Thin Films, Vol 9, pp. 145-261, 1977.

A2 Stegeman G I, Burke J J and Hall D G, "Surface-Polariton like Waves Guided by Thin, Lossy Metal Films", Optics Letters, Vol 8, No 7, pp. 383-385, July 1983.

A3 Burke J J, Stegeman G I and Tamir T, "Surface-Polariton-Like Waves Guided by Thin, Lossy Metal Films", Physical Review B, Vol 33, No 8, pp.5186-5201, April 1986.

A4 Zervas M N, "Non-Linear and Resonance Effects in Fibre-Optic Components", PhD Thesis, Dept. of Electronic and Electrical Engineering,
University College London, July 1989, pp. 90-162.

A5 Welford K, "Surface Plasmon-Polaritons and Their uses", Optics and Quantum Electronics, Vol 23, pp. 1-27, 1991.

A6 Raether H, "Excitation of Plasmons and Interband Transitions by Electrons," Springer Tracts in Modern Physics 88, Springer Verlag (Berlin Heidelberg New York) 1980.

A7 Raether H, "Surface Plasmons," Springer Tracts in Modern Physics 111, Springer Verlag (Berlin Heidelberg New York London Paris Tokyo) 1988.

A8 Sambles J R, Bradberry G W and Yang F, "Optical excitation of surface plasmons: An introduction," Contemporary Physics, 32 pp.173-183, 1991.

A9 Zervas M N, "Surface plasmon-polariton waves guided by thin metal films," Optics Letters 16, pp.720-722, 1991.

B. Surface-Plasmons and Optical Fibres:

B1 Stewart G, Johnstone W, Culshaw B and Hart T, "Surface Plasmon Resonances in Thin Metal Films for Optical Fibre Devices", OFS'88, pp. 328-331, Louisiana, U.S.A., January 1988.

B2 Zervas M N and Giles I P, "Optical-Fibre Surface-Plasmon-Wave Polarizers with Enhanced Performance". Electronics Letters, Vol 25, No 5, pp. 321-323, March 1989.

B3 Zervas M N, "Surface Plasmon-Polariton Fiber-Optic Polarizers Using Thin Nickel Films", IEEE Photonics Tech. Letters, Vol 2, No 4, pp.253-256, April 1990.

B4 Johnstone W, Stewart G, Hart T and Culshaw B, "Surface Plasmon Polaritons in Thin Metal Films and Their Role in Fiber Optic Polarizing Devices", J Lightwave Tech, Vol 8, No 4, pp. 538-533, April 1990.

B5 Zervas M N and Giles I P, "Performance of Surface Plasma-Wave Fiber-Optic polarizers", Optics Letters, Vol 15, No 9, pp. 513-515, May 1990.

B6 Zervas M N, "Surface Plasmon-Polariton Fiber-Optic Polarizers Using Thin Chromium Films", IEEE Photonics Tech Letters, Vol 2, No 8, pp. 597-599, August 1990.

B7 Villuendas F, and Pelayo J, "Optical Fibre Device for Chemical Sensing Based on Surface Plasmon Excitation", Sensors and Actuators, A21-23, pp. 1142-1145, 1990.

B8 Khosravi H, Tilley D R and Loudon R, "Surface Polaritons in Cylindrical Optical Fibers", J. Opt. Soc. Am. A, Vol 8, pp. 112-122, January 1991.

B9 Carey S and Johnstone W, "Characterisation of Surface Plasmon wave polarising Devices", Electron. Letters, Vol 27, No 11, pp. 988-990, May 1991.

B10 Zervas M N, "Surface plasmon-polariton waves guided by thin metal films," Optics Letters, 16 pp. 720-722, 1991.

B11 Al-Bader S J and Imtaar M, "TM-polarized surface-plasma modes on metal-coated dielectric cylinders", J. Lightwave Technology, Vol 10, No 7, pp. 865-872, July 1992.

B12 Zakhidov E A, Zakhidova M A, Kasymdzhanov M A and Khabibullaev P K, "Surface enhanced raman scattering by biomolecules in fiber-optic structures with metallic cover", XIIIth International Conference on Raman Spectroscopy, post-deadline paper, pp. 134-135, Wurzburg, Germany, September 1992.

B13 Sifam Ltd – Fibre Optics Division, "Fibre Optic Product Data Sheets", May 1991, Torquay, Devon England.

C. Surface plasmons : General publications and applications:

C1 Pines D, "Collective Energy Losses in Solids", Rev. of Modern Physics, Vol 28, No 3, pp. 194-186, July 1956.

C2 Walker C T, and Slack G A, "Who Named the ON's", American Journal of Physics, Vol 28, No 12, pp. 1380-1385, Dec 1970.

C3 Claus R, Mertem L, and Brandmüller J, "Light Scattering by Phonon-Polaritons", Springer Tracts in Modern Physics, Springer-Verlag, 1975.

C4 Sarid D, "Long-Range Surface Plasma Waves on Very Thin Metal Films", Phys. Rev. Letters, Vol 47, No. 26, pp. 1927-1930, Dec 1981.

C5 Wendler L and Haupt R, "Long-Range Surface Plasmon-Polaritons in symmetric Layer Structures", J. Appl. Phys. Vol 53, No. 3, pp. 3289-3291, May 1986.

C6 Hickernell R K and Sarid D, "Long-Range Surface Magneto Plasmons in Thin Nickel Films", Optics Letters, Vol 12, No 8, pp. 570-572, August 1987.

C7 Schildraut J S, "Long-Range Surface Plasmon Electrooptic Modulator", Applied Optics, Vol 27, No. 21, pp 4587-4590, November 1988.

C8 Yang, F, Bradberry G W and Sambles J R, "Surface Plasmon Observed Using a Scanning Index Method", Optics Communications, Vol 74, No 1,2, pp. 1-4, Dec 1989.

C9 Bruijm H E, Kooyman R P H and Greve J, "Determination of Dielectric permittivity and thickness of a metal layer from a surface plasmon resonance experiment", App. Optics, Vol 29, No 13, pp 1974-1978, May 1990.

C10 Tillim M D and Sambles J R, "Temperature Dependence of Surface Plasmon-Polaritons on Silver", Vacuum, Vol 41, Nos 4-6, pp. 1186-1188, 1990.

C11 Bryan-Brown G P, Sambles J R, Hutley M C, "Polarisation Conversion through the excitation of Surface Plasmons on a metallic grating", Journal of Modern Optics, Vol 37, No. 7, pp. 1227-1232, 1990.

C12 Naoi Y and Fukui M, "Intensity of Surface-Plasmon Polariton Energy transmitted into the air side in an air/Ag-Film/Prism Configuration", Physical Review B, Vol 42, No. 8, pp 5003-5012, September 1990.

C13 Fontana E, Pantell R H and Strober S, "Surface Plasmon Immunoassay", App. Optics, Vol 29, No. 31, pp. 4694-4704, November 1990.

C14 Feibelman P J and Tsuei K D, "Negative Surface-Plasmon dispersion coefficient : A physically illustrative formula", Physical Review B, Vol 41, No 12, pp. 8519-8521, April 1990.

C15 Caldwell M E and Yeatman E M, "Performance Characteristics of Surface Plasmon Liquid Crystal Light Valve", Electronics Letters, Vol. 27, No. 16, pp. 1471-1472, August 1991.

C16 Yang F, Sambles J R and Bradberry G W, "Long-range surface modes supported by thin films," Phys Rev B 44 pp. 5855-5872, 1991.

C17 Bryan-Brown G P, Yang F, Bradberry G W and Sambles J R, "Prism and rating coupling to long-range coupled-surface exciton-polaritons," JOSA B 8, pp. 765-769, 1991.

C18 Craig A E, Olson G A and Sarid D, "Experimental observation of the long-range surface-plasmon polariton," Optics Letters 8, pp. 380-382, 1983.

C19 Innes R A, Welford K R and Sambles J R, "Poynting vector in uniaxially birefringent multilayered system," Liquid Crystals 2, pp, 843-851, 1987.

C20 Yang F, Bradberry G W and Sambles J R, "Long-range surface mode supported by very thin silver films," Phys Rev Lett 66, pp. 2030-2032, 1991.

C21 Yang F, Bradberry G W and Sambles J R, "Long range surface exciton polaritons: New long range surface modes," Modern Physics Letters B 4, pp. 1119-1132, 1990.

C22 Kou E F Y and Tamir T, "Incidence angles for optimized ATR excitation of surface plasmons," Applied Optics 27, pp. 4098-4103, 1988.

C23 Quail J C, Rako J G and Simon H J, "Long-range surface-plasmon modes in silver and aluminium films," Optics Letters 8, pp. 377-379, 1983.

C24 Burton F A and Cassidy S A, "A complete description of the dispersion relation for thin metal film plasmon-polaritons," J Lightwave Technology 8, pp. 1843-1849, 1990.

C25 Kou F Y and Tamir T, "Range extension of surface plasmons by dielectric layers," Optics Letters 12, pp. 367-369, 1987.

C26 Ko D Y K and Sambles J R, "Scattering matrix method for propagation of radiation in stratified media: attenuated total reflection studies of liquid crystals", J. Opt. Soc. Am. A, Vol 5. No 11, pp. 1863-1866, November 1988.

C27 Hulse C A and Knoesen A, "Iterative calculation of complex propagation constants of modes in multilayer planar waveguides", IEEE J. Quantum Electronics, Vol 28, No 12, pp. 2682-2684, December 1992.

C28 Weber W H and McCarthy S L, "Surface-plasmon resonance as a sensitive probe of metal-film properties", Physical Review B, Vol 12, No 12, pp. 5643-5650, December 1975.

C29 Hickel W and Knoll W, "Surface plasmon optical characterization of lipid monolayers at 5 μm lateral resolution", J. Appl. Phys., Vol 67, No 8, April 1990.

C30 Dzhavakhidze P G, Kornyshev A A, Tadjeddine A and Urbakh M I, "Potential dependence of the surface plasmon dispersion relation and the role of adsorption of anions at the electrochemical interface", Electrochimica Acta, Vol 34, No 12, pp. 1677-1680, 1989.

C31 Kovacs G J, "Sulphide formation on evaporated Ag films", Surface Science, Vol 78, pp. L245-L249, 1978.

C32 Dumas P, Dubarry-Barbe J P, Riviere D, Levy Y and Corset J, "Growth of thin alumina film on aluminium at room temperature: a kinetic and spectroscopic study by surface plasmon excitation", Journal de Physique, Tome 44, pp. C10-205 to C10-208, December 1983.

C33 Nylander C, Liedberg B and Lind T, "Gas detection by means of surface plasmon resonance", Sensors and Actuators, Vol 3, pp. 79-88, 1982.

D. Useful references not necessarily concerning surface plasmons:

D1 Digonnet M J F and Shaw H J, "Analysis of a Tunable Single Mode Optical Fiber Coupler", IEEE J. Quantum Electronics, Vol QE-18, No. 4, pp. 746-754, April 1982.

D2 Leminger O G and Zengerle R, "Determination of Single-Mode Fiber Coupler Design Parameters from Loss Measurements", J.Lightwave Technology, Vol. LT-3, No. 4, pp. 864-867, August 1985.

D3 Digonnet M J F, Feth J R, Stokes L F and Shaw M J, "Measurement of the Core Proximity in Polished Fiber Substrates and Couplers", Opt. Letters, Vol 10, No. 9, pp.463-465, September 1985.

D4 Pokrowsky P, "Optical Methods for Thickness Measurements on Thin Metal Films", App. Optics, Vol 30, No. 22, pp. 3228-3232, August 1991.

D5 Culverhouse D, PhD Thesis, University of Kent, Canterbury, UK, Appendix A, "Fabrication of Directional Coupler and Ring resonator"), 1991.

D6 Minelly J, "Field Access Techniques for Single-Mode Fibres", PhD Thesis, Department of Electronics and Computer Science, Faculty of Engineering and Applied Science, University of Southampton, Southampton, UK, November 1989.

D7 Nicholls S T, "Automatic Manufacture of Polished Single-Mode Fibre Directional Coupler", Electron. Lett. Vol. 21, pp 825-826, 1985.

D8 Heffner B L, "Deterministic, analytically complete measurement of polarisation-dependent transmission through optical devices," IEEE Phot Techn Lett, 4 pp. 451-454, 1992.

D9 Ulrich R and Torge R, "Measurement of thin film parameters with a prism coupler," Applied Optics 12, pp. 2901-2908, 1973.

D10 Holland L, "Vacuum deposition of thin films," Chapman and Hall (London) 1963.

D11 Fukui M and Oda K, "Studies of metal film growth through instantaneously observed attenuated total reflection spectra," Applied Surface Science, 33/34 pp. 882-889, 1988.

D12 Yamaguchi T, Yoshida S and Kinbara A, "Continuous ellipsometric determination of the optical constants and thickness of a silver film during deposition," Jap J Appl Phys 8, pp. 559-567, 1969.

D13 Inagaki T, Goudonneet J P, Royer P and Arakawa E T, "Optical properties of silver island films in the attenuated-total-reflection geometry," Applied Optics 25, pp. 3635-3639, 1986.

D14 Marhic M E, Kwan L I and Epstein M, "Optical surface waves along a toroidal metallic guide," Appl Phys Lett 33, pp. 609-611, 1978.

D15 Onodera H, Awai I and Ikenoue J.-I., "Refractive-index measurement of bulk materials: Prism coupling method," Applied Optics 22, pp. 1194-1197, 1983.

D16 Sennett R S and Scott G D, "The structure of evaporated metal films and their optical properties," JOSA 40, pp. 203-211, 1950.

D17 Shaklan S, "Measurement of intermodal coupling in weakly multi-mode fibre optics", Electronics Letters, Vol 26, No 24, pp. 2022-2024, November 1990.

D18 Russell PStJ and Ulrich R, "The grating-fiber coupler as a high resultion spectrometer," Optics Letters, Vol 10, pp. 291-291, 1985.

E. References on physical properties of metals:

E1 Johnson P.B. and Christy R W, "Optical constants of the noble metals," Phys Rev B 6, pp. 4370-4379, 1972.

E2 Weaver J H, Krafka C, Lynch D W and Koch E E, "Optical properties of metals Part II: Noble metals, Aluminum, Scandium, Yttrium, the Lanthanides and the Actinides," Physics Data, ISSN 0344-8401, 1981.

E3 Reale C, "Optical constants of vacuum deposited thin metal films in the near infrared," Infrared Physics, 10 pp. 175-181, 1970.

E4 Palik E D (Editor), "Handbook of optical constants of solids," Academic Press Handbook Series, 1985.

E5 Ordal M A, Long L L, Bell R J, Bell S E, Bell R R, Alexander R W and Ward C A, "Optical properties of Al,Co,Cu,Au,Fe,Pb,Ni,Pd,Pt,Ag,Ti and W in the IR and far IR," Appl Opt, 22 pp. 1099-1119, 1983.

6. ANCILLARY TOPICS

6.1 Planned publications

We are planning to submit at least one theoretical article outlining the design procedure for mode-selective LRSP couplers, and to submit a conference and a short journal paper describing the experimental results (subject to approval from the sponsor).

6.2 Names of participating professionals

Sergio Barcelos, a PhD student, is the person working full-time on the project, under the guidance of the principal investigator. Other members of the ORC who have contributed to the programme include Dr Chris Lavers, who has given invaluable practical assistance, Dr Michael Zervas who has advised S. Barcelos usefully, and Dr Tim Birks who has assisted on some theoretical matters.

6.3 Interactions with other groups

We have interacted with the group of Prof Roy Sambles at Exeter University on some aspects of the programme. Prof Paras Prasad of SUNY Buffalo was contacted about the possibility of using electrooptic polymers instead of liquid crystals for the tunable device.

6.4 New discoveries, inventions and patents

There have been no notable discoveries, inventions or patent disclosures from the project, although we feel that our understanding (described in this report) of the use and limitations of LRSP modes for mode selection is now very good. Specific applications have concentrated on studying in depth the feasibility of MFSPR couplers as mode-selective taps.

6.5 Additional points

A number of topics discussed in this document are still under study – in particular the modelling of the multi-mode case using the Lorentzian resonance approach and more experiments on the performance of the MFSPR coupler. We would be prepared to report informally on these topics, should interesting developments arise. Progress was considerably slowed owing to the need to move our entire laboratories to a new building, which unfortunately took place in the middle of the 18 month project period. This has not permitted us to explore in quite as much detail as we would have liked the properties of the devices – but nevertheless our conclusion, namely that metal films cannot provide good mode selection, is we believe sound. Since good mode selectivity proved to be unattainable in practice, and a great deal of time was spent on proving this both theoretically and experimentally, there seemed little point in pursuing the dependent goals of tunability and reducing insertion loss.